NYSGI-T-85-003 C3

Report No. 85-1

LOAN COPY ONLY

HYDRAULICS OF RIVER ICE

by Hung Tao Shen

NATIONAL SEA GRANT DEPOSITORY
PELL LIBRARY BUILDING
URI NARRAGANSETT BAY CAMPUS
NARRAGANSETT, RI 02882

Department of Civil and Environmental Engineering
Clarkson University
Potsdam, New York 13676

August, 1985

NYSGI-T-85-003 C3

CIRCULATING COPY
Sea Grant Depository

Hydraulics of River Ice

by

Hung Tao Shen

NATIONAL SEA GRANT DEPOSITORY
PELL LIBRARY BUILDING
URI, NARRAGANSETT BAY CAMPUS
NARRAGANSETT, RI 02882

Report No. 85-1

Department of Civil and Environmental Engineering
Clarkson University
Potsdam, New York

August, 1985

PREFACE

This report summarizes lecture notes for a short course presented by the author at the Institute of Water Conservancy and Hydroelectric Power Research, Academia Sinica and the Ministry of Water Resources and Electric Power, China. The material herein is intended to serve as a summary of the lectures. Due to limitations of space and time, coverage of many subjects is brief or even omitted. Reader should refer to selected references for more detailed information.

The author would like to acknowledge support provided for his research on river ice hydraulics by the U.S. Army Cold Regions Research and Engineering Laboratory; the New York Sea Grant Institute, and the Great Lakes Environmental Research Laboratory, both of NOAA, Department of Commerce; the St. Lawrence Seaway Development Corporation, Department of Transportation; and the National Science Foundation. This report is prepared with partial support from the U.S. Army Cold Regions Research and Engineering Laboratory, through a Joint Graduate Research Program in Ice Engineering under Contract No. DACA89-84-K-0008.

Appreciation is also expressed to many colleagues who have helped the writer's understanding of river ice phenomena through collaboration, discussion and encouragement.

CONVERSION FACTORS

Length:

12 in = 1 ft
2.54 cm = 1 in
$1\mu m = 10^{-6}m = 10^{-4}cm$
1 in = 0.0254m
1 ft = 0.3048m
1 mi = 1.60934 km

Area:

$1\ in^2 = 645.16\ mm^2$
$1\ ft^2 = 0.092903\ m^2$
$1\ sq.\ mile = 2.58999\ km^2$

Volume:

$1\ in^3 = 1.63871 \times 10^{-5}\ m^3$
$1\ ft^3 = 0.0283168\ m^3$
$1\ gal = 231\ in^3 = 0.004546092\ m^3$

Mass:

$1\ kg = 2.205\ lb_m$
$1\ slug = 32.16\ lb_m$
$454\ g = 1\ lb_{fm}$

Density:

$1\ lb_m/in^3 = 2.76799 \times 10^4 kg/m^3$
$1\ lb_m/ft^3 = 16.0185\ kg/m^3$

Force:

$1\ dyn = 2.248 \times 10^{-6}\ lb_f$
$1\ lb_f = 4.448\ N$
$10^5\ dyn = 1\ N$

Pressure:

$1\ atm = 1.01325 \times 10^5\ N/m^2$
$1\ lb_f/in^2 = 6894.76\ N/m^2$
$1\ atm = 14.696\ lb_f/in^2 = 2116\ lb_f/ft^2$
$1\ atm = 1.01325 \times 10^5\ N/m^2$
$1\ in\ Hg = 70.73\ lb_f/ft^2$

CONVERSION FACTORS (cont.)

Energy:

1 kWh = 3413 Btu
1 hp·h = 2545 Btu
1 Btu = 252 cal
1 Btu = 778 $ft \cdot lb_f$
1 erg = 10^{-7} J
1 Btu = 1055.06 J
1 $ft \cdot lb_f$ = 1.35582 J
1 cal(15°C) = 4.1855 J

Power:

1 hp = 745.7 W
1 Btu/h = 0.293 W

Heat Flux:

1 $Btu/h \cdot ft^2$ = 3.15372 W/m^2
1 Btu/h·ft = 0.96128 W/m

Thermal Conductivity:

1 $Btu/h \cdot ft \cdot °F$ = 1.730278 $W/m^2 \cdot °C$

Heat Transfer:

1 $Btu/h \cdot ft^2 \cdot °F$ = 5.67683 $W/m^2 \cdot °C$

Thermal Conductivity:

1 cal/s·cm·°C = 242 Btu/h·ft·°F
1 W/cm·°C = 57.79 Btu/h·ft·°F

Viscosity:

1 centipoise = 2.42 $lb_m/hr \cdot ft$
1 $lb_f \cdot s/ft^2$ = 32.16 $lb_m/s \cdot ft$

NOMENCLATURE (96)

Agglomerate (块集(冰))	- An ice cover of floe formed by the freezing together of various forms of ice.
Anchor Ice (錨冰、底冰)	- Submerged ice attached or anchored to the bottom, irrespective of the nature of its formation.
Anchor Ice (錨冰堰) Dam	- An accumulation of anchor ice which acts as a dam and raises the water level.
Break-up (解凍始(期)) Initiation	- Time of definite breaking or movement of ice due to melting, current or rise of water level.
Beginning of (封凍始(期)) Freeze-up	- Date on which ice forming stable winter ice cover first observed on the water surface.
Black Ice (冰淞.透明冰)	- Transparent ice formed in rivers and lakes.
Border Ice (岸冰)	- An ice sheet in the form of a long border attached to the shore.
Brash Ice (碎冰)	- Accumulations of floating ice made up of fragments not more than 2 m across; the wreckage of other forms of ice
Break-up (解凍)	- Disintegration of ice cover.
Break-up (解凍日期) Date	- The date on which a body of water is first observed to be entirely clear of ice, and remains clear thereafter
Break-up (解凍歷時) Period	- Period of disintegration of an ice cover.
Candle Ice (烛状冰(冰烛)	- Rotten columnar-grained ice.
Columnar (柱状冰(冰柱)) Ice	- Ice consisting of columnar shaped grain. The ordinary black ice is usually columnar-grained.

Consolidated(堅 冰 蓋) Ice Cover - Ice cover formed by the packing and freezing together of floes, brash ice and other forms of floating ice.

Duration of (冰 封 期) Ice Cover - The time from freeze-up to break-up of an ice cover.

Floating Ice(浮 冰) - Any form of ice floating in water.

Floc (絮 狀 冰) - A cluster of frazil particles.

Flooded Ice (覆 水 冰) - Ice which has been flooded by melt water or river water and is heavily loaded by water and wet snow.

Fracture (破 裂) - Any break or rupture formed in an ice cover or floe due to deformation.

Frazil (針粒狀冰屑冰) - Fine spicules, plates or discoids of ice suspended in water. In rivers and lakes it is formed in supercooled turbulent waters.

Frazil Slush(冰 花) - An agglomerate of loosely packed frazil which floats or accumulates under the ice cover.

Freeze-up (封 凍 日 期) Date - The date on which the water body is first observed to be completely frozen over.

Freeze-up (封凍歷時) Period - Period of initial formation of an ice cover.

Granular Ice(球粒狀冰) - Ice made of granular ice grains.

Hanging (冰 壩) (ice) Dam - A mass of ice composed mainly of slush or broken ice deposited under an ice cover.

Ice Boom (防 冰 柵) - Floating structure designed to retain ice.

Ice Bridge (冰 橋) - A continuous ice cover of limited size extending from shore to shore like a bridge.

Ice Clearing(冰 消) - Break-up prior to full melting.

Ice Cover (冰 蓋) - A significant expanse of ice of any possible form on the surface of a body of water.

Ice Edge (冰緣,冰迴) - The demarcation at any given time between the open water and ice of any kind, whether static or dynamic. It may be termed compacted or diffuse.

Ice Floe (浮 冰) - Free floating piece of ice greater than 1 meter in extent.

Ice Jam (冰 塞) - An accumulation of ice at a given location which, in a river, restricts the flow of water.

Ice Jamming (冰堵,冰卡) - The process of accumulation of ice to form an ice jam.

Ice Needle (冰 針) - A small needle-like ice crystal formed under certain nucleation conditions.

Ice Run (流 冰) - Flow of ice in a river. An ice run may be light or heavy, and may consist of frazil, anchor, slush or sheet ice.

Ice Sheet (冰 層) - A smooth continuous ice cover.

Pancake Ice (薄餅狀冰) - Circular flat pieces of ice with a raised rim; the shape and rim are due to repeated collisions.

Rotten Ice (融冰,爛冰) - Ice in an advanced stage of disintegration.

Rough Ice (崎岖冰,粗糙冰) - General term for ice covers with rough surfaces.

Skim Ice (粥 樣 冰) - Initial thin layer of ice on a water surface.

Slush Ball (流冰球,冰花球) - The result of extremely compact accretion of snow, frazil and ice particles. This is produced by either wind and wave action along the shore lakes or in long stretches of turbulent flow in rivers.

Slush (冰 花 流) - Ice run composed mainly of slush ice.
Ice Run

Snow Ice (雪 冰) - Ice that forms when snow slush on an ice cover freezes. It has a white appearance due to presence of air bubbles.

Snow Slush (雪泥、濕雪)	- Snow which is saturated with water on ice surfaces, or as a viscous mass floating in water after a heavy snowfall.
Thermal (溫縮冰縫) Crack	- Crack caused by contraction of ice due to change in temperature.
Unconsolidated(未固結的冰蓋) (Ice Cover)	- Loose mass of floating ice.

CONTENTS

I. INTRODUCTION

Surface water bodies in a substantial portion of the populated regions of the world freeze either totally or partially in the winter. Figure 1 shows the area of ice cover and its duration in terms of navigability for the cold regions of the Northern Hemisphere. The presence of ice can seriously interfere with the utilization of lakes and rivers for power generation, navigation, water supply, etc. Ice and its effects are important considerations in the design, operation, and maintenance of hydraulic engineering facilities. In rivers ice can cause serious problems by the damage it does to hydraulic structures, by the flooding that often accompanies ice jams, by interference with hydropower operations, and by impeding inland navigations. Despite the cost associated with the interference caused by river ice, relatively little effort has been given by engineers in dealing with these problems versus the level of study devoted to rivers under ice free conditions. Nevertheless, substantial progress has been made in the last two decades. A few treatises on ice engineering exist, including those of Barnes (12), Michel (56,57), Pivovarov (74), Shulyakovskii (91), and Ashton (11). Several review papers and reports on river ice have been published (6,8,9,95,105). This report will review the hydraulic aspects of river ice with an emphasis on the formulation and modelling of processes that are involved.

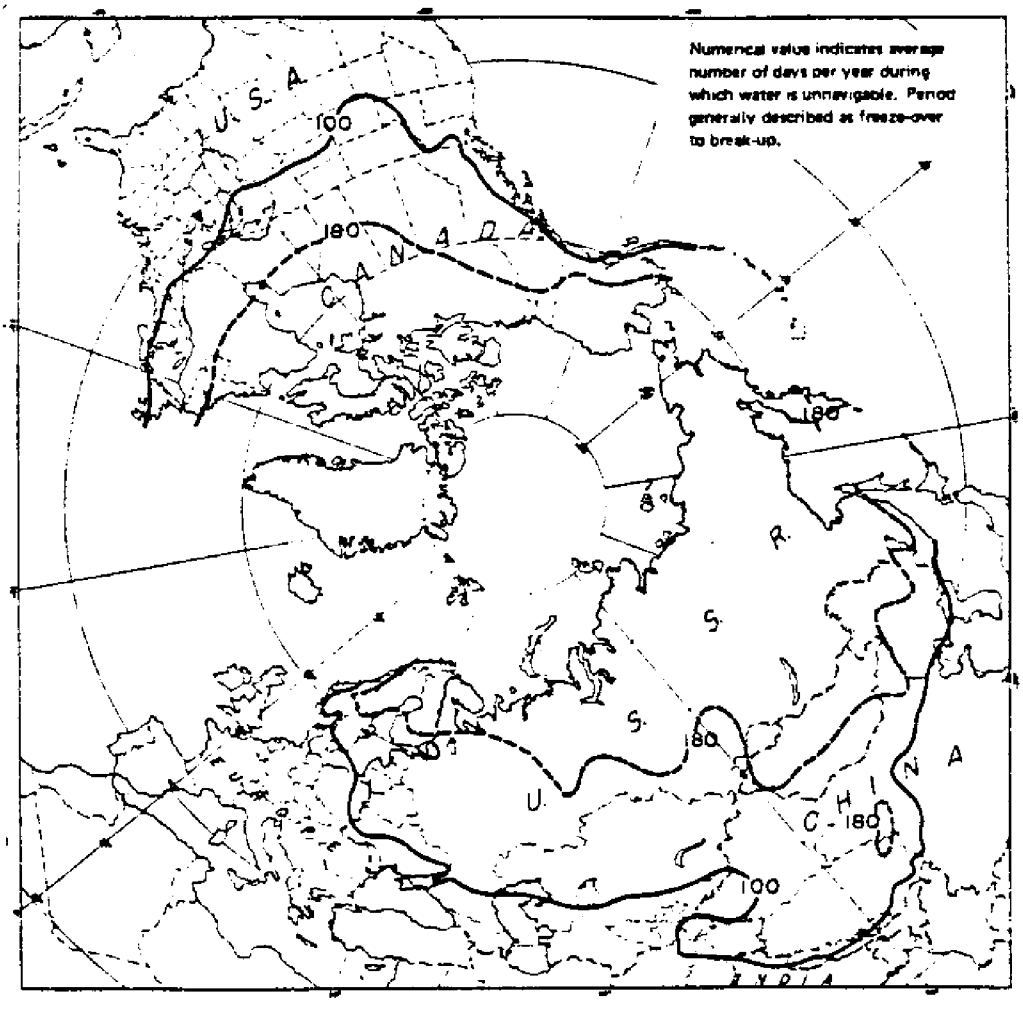

Figure 1. Average number of days during the year in which water is unnavigable (13).

II. HEAT EXCHANGE PROCESSES

A river's thermal-ice condition is affected by heat exchanges through interfaces among the atmosphere, ice cover, river water, and channel bed. A brief summary of the various heat exchange processes follows.

Energy Exchanges at Air-Ice or Air-Water Interfaces.

Heat exchanges with the atmosphere vary with meteorological conditions (65,88). The surface heat exchange process consists of five major components: (1) Net solar (shortwave) radiation, ϕ_s; (2) longwave radiation, ϕ_b; (3) evapo-condensation, ϕ_e; (4) sensible heat exchange, ϕ_c; and (5) precipitation, ϕ_r.

Shortwave Radiation. - The incoming shortwave radiation at the air-ice or air-water interface can be written as

$$\phi_{ri} = [a-b(\Phi-50)](1-0.0065C_c^2) \qquad (1)$$

in which ϕ_{ri} = incoming shortwave radiation, in cal-cm^{-2}-day^{-1}; Φ = latitude in degrees; C_c = cloud cover in tenths; and a, b = constants which represent variations of solar radiation under a clear sky. Average monthly values for a and b are given in Table 1. Since part of the solar radiation reaching the water surface is reflected back into the atmosphere, the net solar radiation, ϕ_s, in cal-cm^{-2}-day^{-1}; can be written as

$$\phi_s = (1 - \alpha)\phi_{ri} \qquad (2)$$

TABLE 1.-Values of a and b in Eq. 1.

Month	a, in cal-cm^{-2}-day^{-1}	b
Dec.	100	8.2
Jan.	142	11.0
Feb.	228	11.2
Mar.	394	12.7
Apr.	554	8.4

in which α = a coefficient approximately equal to 0.1 for the water's surface. Dingman and Assur (38) suggested the following formula for calculating ϕ_s:

$$\phi_s = \phi_{ri} - (0.108\phi_{ri} - 6.766 \times 10^{-5}\phi_{ri}^2) \quad (3)$$

For the ice surface, the value of the albedo, α, in Eq. 2 is dependent on the material behavior of the ice cover. Based on empirical curves developed by Krutskih, et al. (52) for snow-free sea ice in the Arctic, Wake and Rumer (106) proposed the following expressions:

$$\alpha = \alpha_i \quad ; \quad \text{for } T_a \leq 0^oC \quad (4)$$

$$\alpha = \alpha_a + (\alpha_i - \alpha_a)e^{-\psi T_a} \quad ; \quad \text{for } T_a > 0^oC$$

in which α_i, α_a, and ψ = empirical constants; and T_a = air

temperature in degrees Celsius. Bolsenga (21) reported values of albedo for Great Lakes ice covers, and observed that the albedo varies with surface temperatures. For uneven surfaces, the albedo also varies with solar latitude. Table 2 gives albedo values reported by Bolsenga for various ice conditions.

TABLE 2. Albedo of Great Lakes Ice (21)

Ice Type	Albedo, as a percentage
Clear lake ice (snow free)	10
Bubbly lake ice (snow free)	22
Ball ice (snow free)	24
Refrozen pancake (snow free)	31
Slush curd (snow free)	32
Slush ice (snow free)	41
Brash ice (snow between blocks)	41
Snow ice (snow free)	46

The penetration of shortwave radiation into the ice cover can be considered as an internal heat source. The vertical distribution of the intensity of monochromatic shortwave radiation can be described by the Bouguer-Lambert exponential law (43,90).

$$\phi_p = \phi_s e^{-\tau_i z} \tag{5}$$

in which ϕ_p = intensity of the shortwave radiation at depth z; τ_i = a bulk extinction coefficient which varies between 0.004 cm^{-1} and 0.07 cm^{-1}. The extinction coefficient is strongly wavelength dependent so that the solar heating in ice cannot be represented by a simple exponential law with a constant bulk

extinction coefficient (43,10). However, since ice thickness computations usually do not consider the vertical distribution of solar heating in ice, a simple exponential law with a constant bulk extinction coefficient may be used.

Based on Eq. 5, the amount of shortwave radiation that penetrates into the water underneath an ice cover is

$$\phi_{sp} = \beta_i \phi_s e^{-\tau_i \theta} \qquad (6)$$

in which β_i = a fraction of absorbed solar radiation that penetrates through the ice-water interface. Due to the small difference in the refractive indices of ice and water, the value of β_i can be taken to be 1.0 (69).

Longwave Radiation. - The longwave, or terrestrial, radiation is the combination of the longwave radiation emitted from the water surface or the ice cover, ϕ_{bs}, and the net atmospheric thermal radiation absorbed by the water body, ϕ_{bn}. Based on the Stefan-Boltzman law of radiation, modifed to account for the emissivity of the body's surface, ϕ_{bs} can be represented by

$$\phi_{bs} = \varepsilon \sigma T_{sk}^4 \qquad (7)$$

in which σ = the Stefan-Boltzman constant, 1.171×10^{-7} cal-cm^{-2}-day^{-1} ^{o}K^{-4}; T_{sk} = water or ice surface temperature, in degrees Kelvin; and ε = emissivity of the surface, assumed to be 0.97 for both the water and the ice surfaces.

The atmospheric radiation under clear skies, ϕ_{bc}, can be

estimated by considering the atmosphere as a gray body:

$$\phi_{bc} = \varepsilon_a \sigma T_{ak}^4 \tag{8}$$

in which T_{ak} = air temperature, in degrees Kelvin; and ε_a = emissivity of the atmosphere. The Brunt formula (65) gives

$$\varepsilon_a = c + d\sqrt{e_a} \tag{9}$$

in which e_a = vapor pressure of air at the temperature T_{ak}, in millibars; and c and d = empirical constants, 0.55 and 0.052, respectively.

Under cloudy skies, water and ice particles at the bottom of the clouds emit additional radiation. Using Bolz's formula the atmospheric radiation under cloudy skies, ϕ_{ba}, can be represented by

$$\phi_{ba} = \phi_{bc}\,(1+k_c C_c^2) = \sigma T_{ak}^4\,(c + d\sqrt{e_a})(1 + k_c C_c^2) \tag{10}$$

in which k_c = empirical constant $\simeq$ 0.0017. Considering that the reflectivity of the ice or water surfaces is 0.03, the net atmospheric radiation is

$$\phi_{bn} = 0.97\phi_{ba} \tag{11}$$

in which ϕ_{bn} = net atmospheric radiation, in cal-cm^{-2}-day^{-1}. Combining Eqs. 7 and 11, the effective back radiation becomes

$$\phi_b = \phi_{bs} - \phi_{bn} = 1.1358 \times 10^{-7}[T_{sk}^4 - (1 + k_c C_c^2)(c + d\sqrt{e_a})T_{ak}^4] \quad (12)$$

in which ϕ_b = effective back radiation, in cal-cm^{-2}-day^{-1}.

Evapo-Condensation. - The heat flux from the water surface due to evapo-condensation, ϕ_e, can be estimated by using the Rimsha-Donchenko formula (65)

$$\phi_e = (1.56K_n + 6.08V_a)(e_s - e_a) \quad (13)$$

in which ϕ_e = rate of heat loss due to evaporation, in cal-cm^{-2}-day^{-1}; V_a = wind velocity at 2 m above the water surface in meters per second; e_s = saturated vapor pressure at temperature T_s; and K_n = a coefficient that accounts for the effect of free convection determined by

$$K_n = 8.0 + 0.35(T_s - T_a) \quad (14)$$

in which T_s = river surface temperature; and T_a = air temperature at 2 m above the water surface, in degrees Celsius. Since the existence of an ice cover on the river surface tends to suppress evaporation (88), the heat flux due to evapo-condensation from the ice surface will be considered as a fraction, C_e, of that calculated from Eq. 13, or

$$\phi_e = C_e(1.56K_n + 6.08V_a)(e_s - e_a) \quad (15)$$

Conductive Heat Transfer. - The energy conducted from the

water surface as sensible heat by air can be determined by the Rimsha-Donchenko formula (65)

$$\phi_c = (K_n + 3.9V_a)(T_s - T_a) \quad (16)$$

in which ϕ_c = rate of conductive heat loss, in cal-cm^{-2}-day^{-1}. Similar to the evapo-condensation flux, a coefficient, C_c, is introduced in Eq. 16 when the river surface is covered by ice, i.e.

$$\phi_c = C_c(K_n + 3.9V_a)(T_s - T_a) \quad (17)$$

Heat Loss Due to Snow Fall. - Heavy snow fall during the ice formation period can increase the amount of ice in the river and affect the ice cover formation significantly. The heat loss due to snow falling on the water surface can be estimated from:

$$\phi_r = A_{sn} [L_i + c_i(T_s - T_a)] \quad (18)$$

in which, A_{sn} = the mass rate of snow fall per unit area of water surface; L_i = the latent heat of fusion of ice, 80 cal g^{-1}; and c_i = specific heat of ice, 1.0 cal g^{-1} ^{o}C^{-1}. A_{sn} can be estimated from the visibility by:

$$A_{sn} = 7.85\ V_p^{-2.375} \quad (19)$$

in which, V_p = the visibility in km; and A_{sn} is in the unit of g

$cm^{-2}day^{-1}$.

Turbulent Heat Transfer from Water to Ice Cover.

The turbulent heat transfer from the flowing river water to the ice cover has significant effects on the thickness of an ice cover (7). The heat flux from the water to the ice cover can be represented by

$$q_{wi} = h_{wi}(T_w - T_f) \tag{20}$$

in which q_{wi} = heat flux from the water to the ice cover; h_{wi} = heat transfer coefficient, in cal cm^{-2} day^{-1} $^oC^{-1}$; T_w = water temperature, in degrees Celsius; and T_f = the freezing point of water, 0^oC. By considering the ice-covered river flow as a smooth-walled closed-conduit turbulent flow, the turbulent heat flux can be formulated as (46):

$$N_u = C\ R^{0.8}P_r^{0.4} \tag{21}$$

where, N_u = Nusselt Number, $h_{wi}R/k_w$; P_r = Prandtl Number, $\rho\nu_w C_p/k_w$ = 13.6 for water near 0^oC; C_p = specific heat of water, 1.0 cal g^{-1} $^oC^{-1}$; C = empirical coefficient approximately 0.023; R_e = Reynolds Number, UR/ν_w; k_w = thermal conductivity of water, 0.552 W m^{-1} $^oC^{-1}$; ν_w = viscosity of water, 1.788 x 10^{-6} m^2 s^{-1}; and R = hydraulic radius. The heat transfer coefficient can be evaluated (7,8,9) by the following equation:

$$h_{wi} = C_{wi} \frac{U^{0.8}}{d_w^{0.2}} \tag{22}$$

in which U = flow velocity in meters per second; d_w = flow depth in meters; and C_{wi} = 1622 W $sec^{0.8}$ $m^{-2.6}$ $^oC^{-1}$ (0.2 Btu $hr^{-0.2}$ $ft^{-2.6}$ $^oF^{-1}$). Laboratory and field investigations indicate that the coefficient C_{wi} may vary with the resistance of the ice cover (46,24). A refined form of Eq. 22, based on the formulation of Petukhov and Popov (73), is

$$h_{wi} = \frac{2k_w}{d_w} \frac{(f_i/8)\ R_e\ P_r}{1.07+12.7\sqrt{f_i/8}\ (P_r^{2/3}-1)} \tag{23}$$

in which, f_i = friction factor of the ice cover.

Bed Heat Influx

In ice-covered rivers, the heat exchange at the bed, q_{gw}, is an important component of the river's heat budget. O'Neil and Ashton (63) developed a procedure for analyzing heat transfer at the channel bottom by considering one-dimensional heat conduction in the channel bed. Expressing the normal water temperature during a year as a sinusoidal function, which intercepts 0°C at times t_1 and t_2:

$$T_w(t) = \begin{cases} \bar{T}_w + a \sin(2\pi t/T_y) & , \quad t \leq t_o \text{ and } t \geq t_2 \\ 0 & , \quad t_1 \leq t \leq t_2 \end{cases} \tag{24}$$

in which, T_y = the period, 1 year; and $\bar{T}_w$ and a = the mean and amplitude of the sinusoidal function, respectively. The nondimensional river bottom temperature gradient at the bed/water interface can be obtained as shown in Figure 2. The

dimensionless variables in Figure 2 are defined as

$$(\theta, \xi, r) \equiv \left(\frac{T_b - \bar{T}_w}{a} \quad , \quad \frac{y_b}{\sqrt{KT_y}} \quad , \quad \frac{\bar{T}_w}{a}\right) \tag{25}$$

in which; y_b = depth of the soil from the bed/water interface, T_b = temperature in the bed; $K = k/\rho_b C_b$ = thermal diffusitivity of soil; in which, k, ρ_b, and C_b = thermal conductivity, density and heat capacity of the bed material (50). The actual bed heat flux, $k\partial T_b/\partial y_b\big|_{y_b=0}$, can be determined from the value of $\partial\theta/\partial\xi$ obtained from curves in Figure 2.

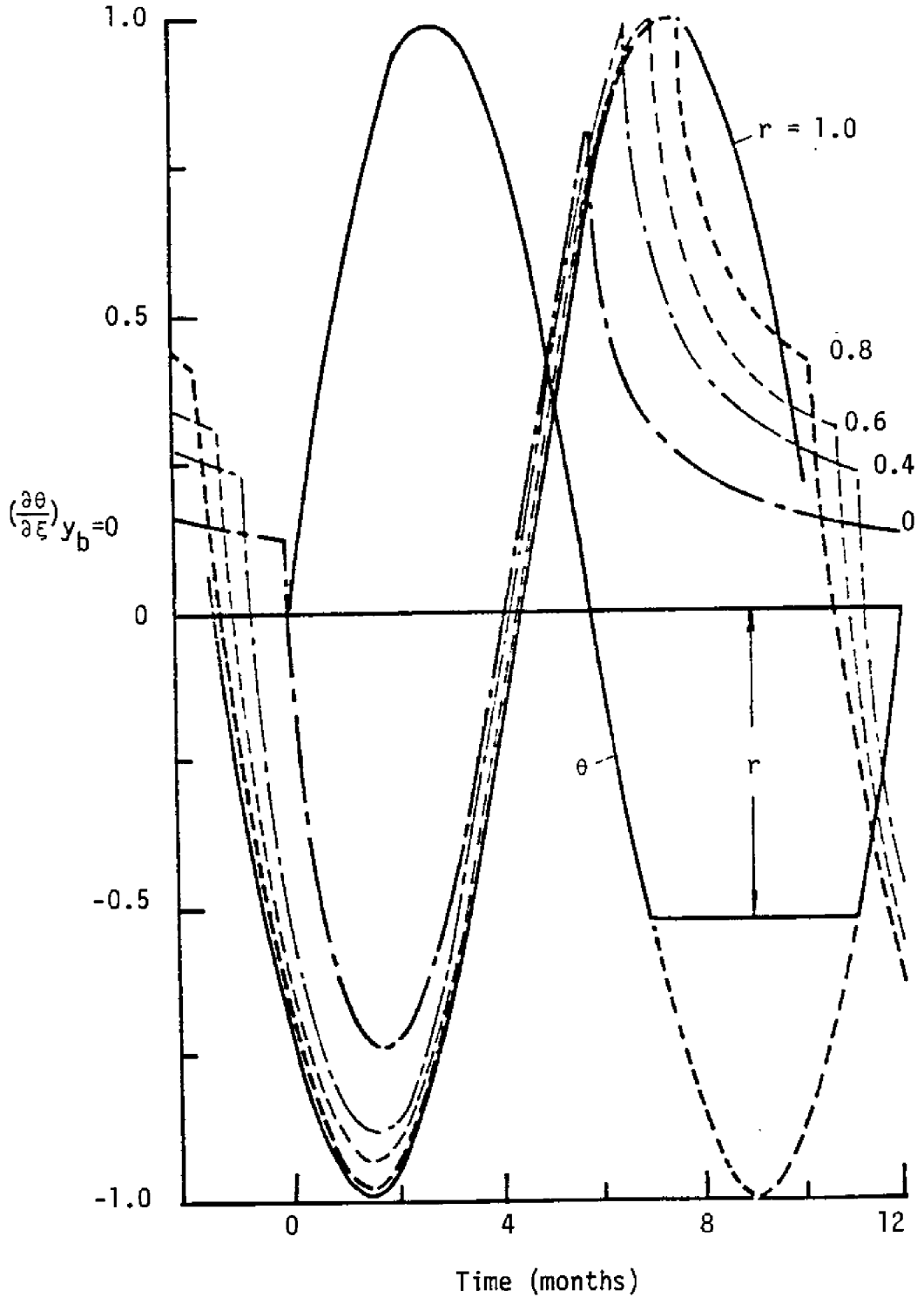

Figure 2. Nondimensional river bottom temperature gradient, evaluated at the bed/water interface, as a function of time and r. The nondimensional river bottom temperature θ is also shown (63).

III. THERMAL-ICE REGIME

Thermal and ice conditions in rivers are strongly influenced by the ambient weather conditions through heat exchanges. Figure 3 shows the normal air and water temperatures of the St. Lawrence River. In this section the winter thermal regime of rivers will be discussed in relation to water temperature distribution, frazil ice formation, and the growth and decay of ice covers.

River Freeze-up

Ice begins to form when the water temperature reaches $0^{\circ}C$ and continues to lose heat to the atmosphere. Under the consideration of complete mixing over the channel cross section, the conservation of thermal energy in a river reach can be represented by a one-dimensional advection-diffusion equation. For water temperature above freezing, this equation can be written (22) as

$$\frac{\partial}{\partial t}\left(\rho C_p A T_w\right) + \frac{\partial}{\partial x}\left(Q\rho C_p T_w\right) = \frac{\partial}{\partial x}\left(AE_x \rho C_p \frac{\partial T_w}{\partial x}\right) + B\Sigma\phi \qquad (26)$$

in which A = cross-sectional area of river; B = channel width; Q = river discharge; ρ = density of water; C_p = specific heat of water; E_x = longitudinal dispersion coefficient; x = distance along the river; and $\Sigma\phi$ = net heat influx per unit surface area of the river.

A few freeze-up forecast models exist (87) for predicting the time at which the water temperature at a river station drops to the freezing point. By assuming that changes in river

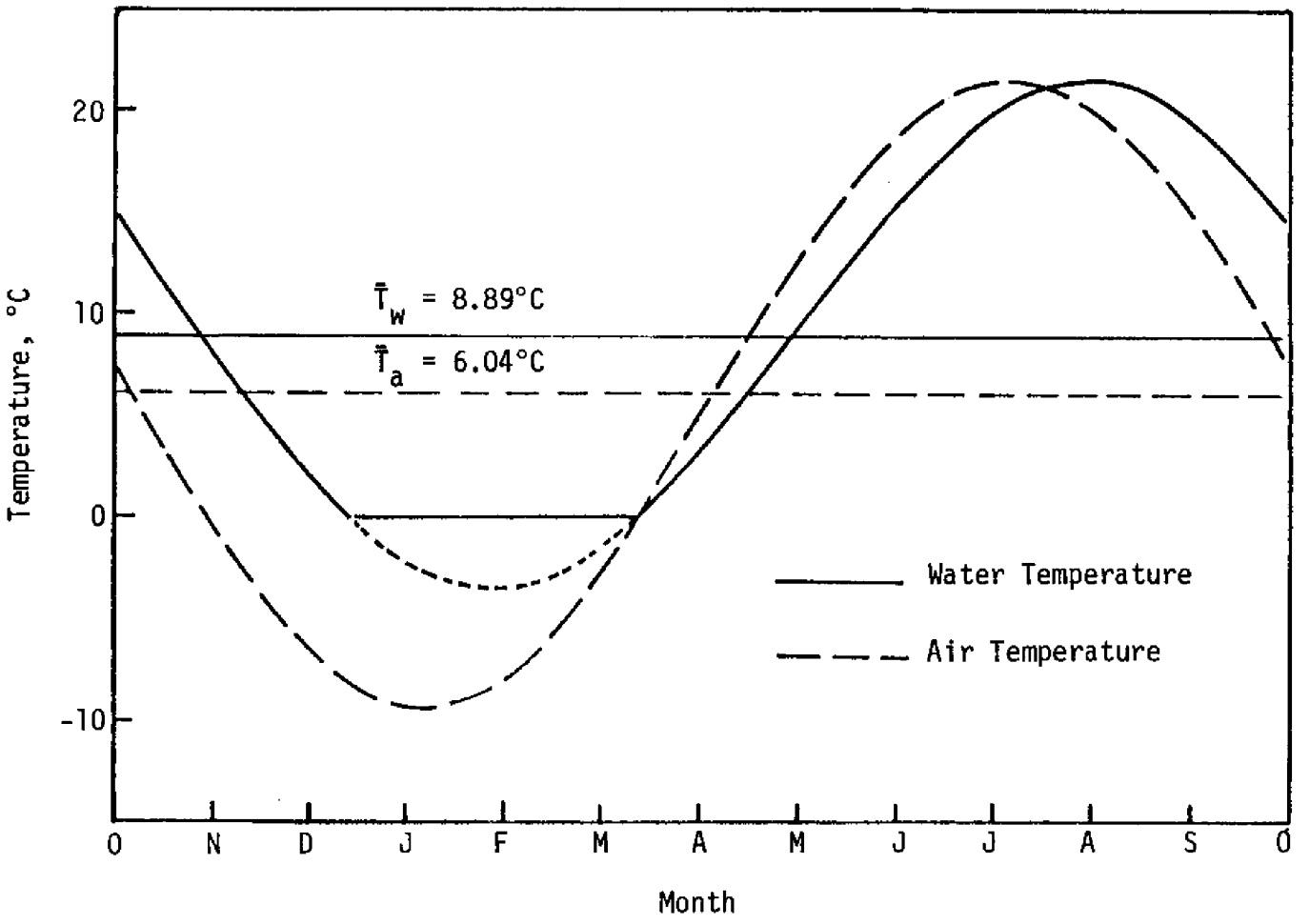

Figure 3. Variation s of air and water temperature in the St. Lawrence River at Massena, N.Y.

discharge are not significant, and neglecting the longitudinal mixing term, Eq. 26 can be reduced to a simplified form

$$\frac{\partial T_w}{\partial t} + V \frac{\partial T_w}{\partial x} = \frac{\Sigma \phi}{\rho C_p d_w} \tag{27}$$

in which, V = the average flow velocity, and d_w = the depth of flow. By representing the heat exchange as a simple linear function in the form of:

$$\Sigma \phi = h_{wa} (T_a - T_w) \tag{28}$$

where h_{wa} = the energy exchange coefficient. For the St. Lawrence River, h_{wa} is approximately equal to 46.4 cal $cm^{-2} day^{-1}$ $^oC^{-1}$. By representing the air temperature T_a as a combination of normal air temperature approximated by the first harmonic of the Fourier series with a period of one year and the short-term variations, a freeze-up forecasting scheme has been developed based on an analytical solution of Eqs. 27 and 28 (87). The short-term variations in air temperature can be obtained from the weather forecast. This scheme has been applied to the upper St. Lawrence River, and is shown to be capable of accurately forecasting freeze-up.

Frazil Ice

Frazil ice forms in supercooled turbulent water. Frazil suspension consists of fine spicule, plate or discoid crystals. Present understanding on the formation of frazil ice has been summarized by Osterkamp (64) and Daly (35). Figure 4 shows the

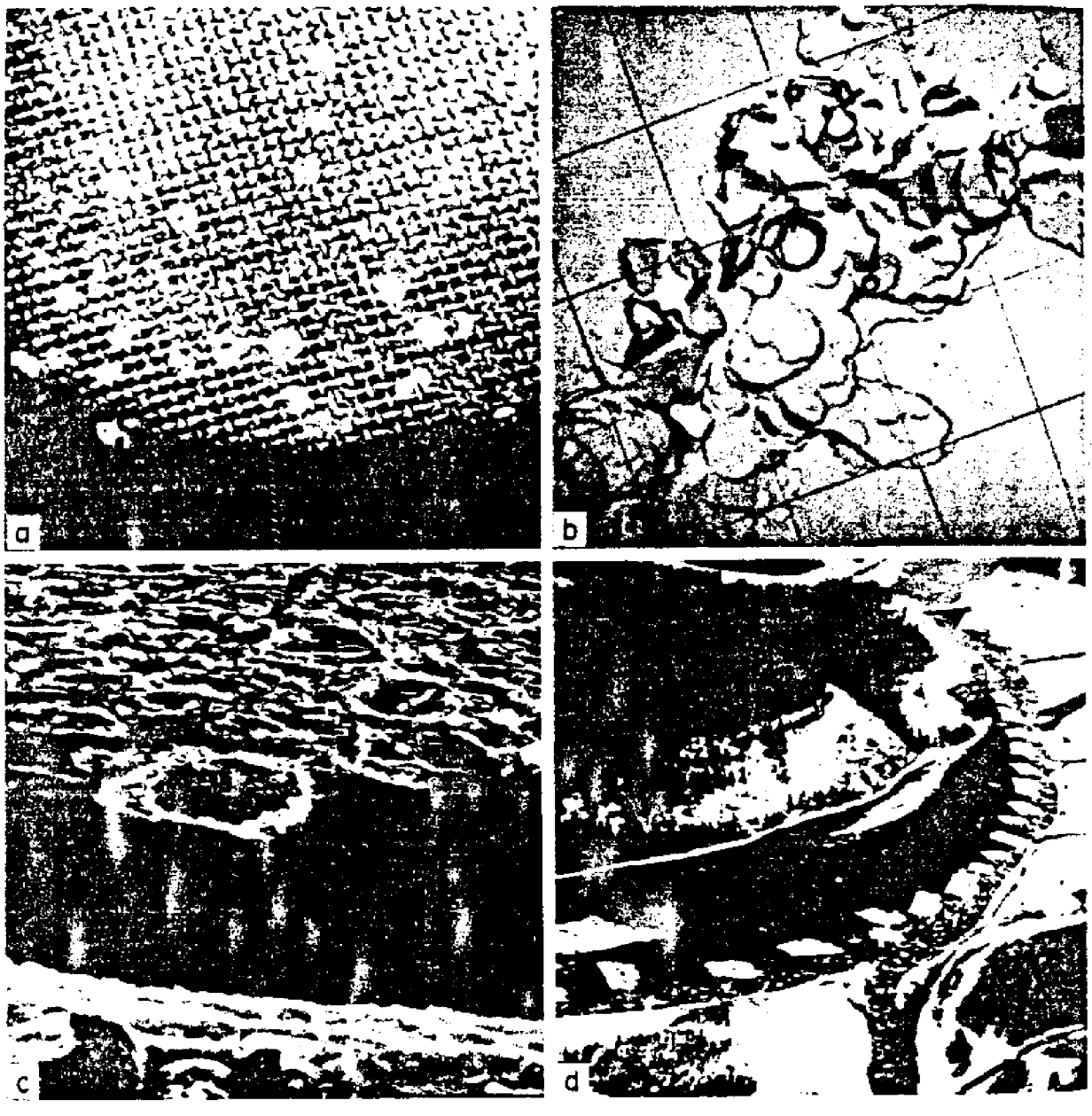

Figure 4. Frazil ice: (a) Initial individual platelets, (b) frazil flocs, (c) frazil pans, (d) an initial ice cover resulting from frazil accumulation (64).

different stages of the evolution of frazil ice in rivers. When the water temperature drops to the freezing point, further cooling, usually by a few hundreths of a degree, causes frazil ice to form in the river. At the supercooled condition, the frazil ice crystals are in their active state of growth. Active frazil ice is found to adhere to nearly any object submerged in the water. Frazil ice blockage of water intakes is a common problem in northern rivers. The temporal variation in water temperature for a constant rate of surface heat loss during the supercooling and frazil formation is typically as shown in Fig. 5. The initial cooling from time t_e to t_n is governed by the surface heat loss. At t_n initial nucleation begins and the cooling rate decreases as frazil ice is being produced. The temperature reaches its maximum depression ΔT_m before asymptotically approaching a residual supercooling temperature ΔT_r. Flume experiments indicated that the values of ΔT_r approaches zero at a large turbulence level (30,31). In general the rate of change of the water temperature of a water mass M_w can be determined using an energy budget analysis:

$$\frac{dT_w}{dt} = \frac{-\phi^*}{C_p M_w} \qquad \text{when } t < t_n \qquad (29)$$

$$\frac{dT_w}{dt} = (L_i \frac{dM_i}{dt} - \phi^*)/[C_p(M_w - M_i)] \qquad \text{when } t > t_n \qquad (30)$$

in which, ϕ^* = net rate of heat loss from the water mass, L_i = latent heat of fusion of ice (80 cal/g), M_i = mass of ice formed. Since frazil ice concentration in rivers is usually on

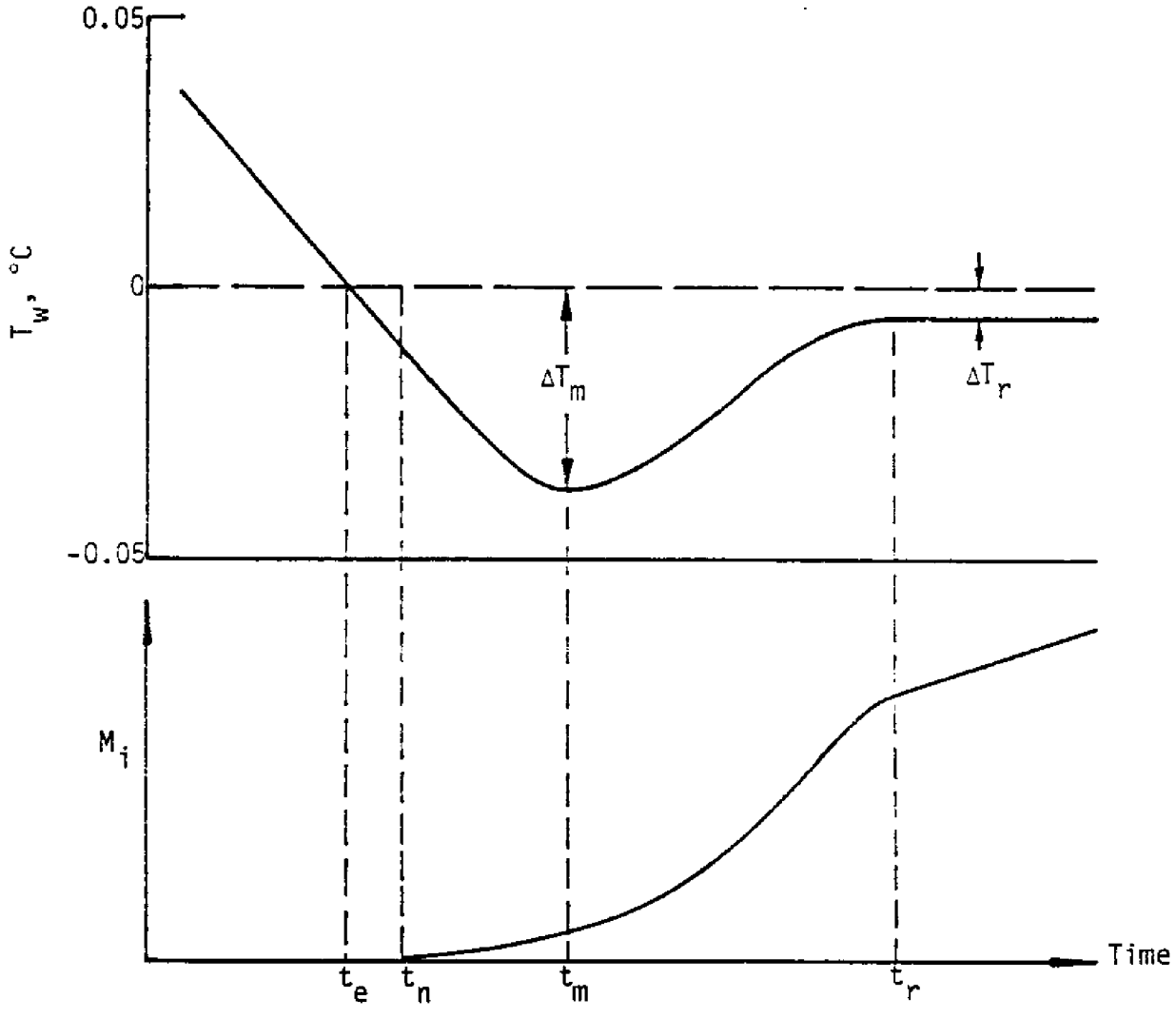

Figure 5. Schematic tremporal history of water temperature and total ice mass produced in water (64).

the order of a few percent or less, one can assume $M_i << M_w$. Neglecting the effect of dT_w/dt during the short period $t_n<t<t_r$, Eq. 30 gives

$$\frac{dM_i}{dt} = \frac{\phi^*}{L_i} \tag{31}$$

For a given river reach at freezing point the rate of ice production can then be estimated by

$$\frac{dQ_i}{dt} = \frac{-\Sigma\phi A_s}{\rho_i L_i} \tag{32}$$

where, A_s = surface area of the river reach, Q_i = volume rate of ice production. Figure 6 shows the total ice production per unit open water area versus the total freezing degree-day of the winter for the St. Lawrence River (78). Recognizing the thermal energy per unit volume in a frazil-laden water as $-\rho_i L_i C_i$, Eq. 26 can be used to determine the concentration of frazil ice, C_i, by replacing $\rho C_p T_w$ with $-\rho_i L_i C_i$.

While the general nature of frazil ice formation can be described by the dynamic balance of the heat loss from the water to the ambient environment and the latent heat released by the growing frazil ice crystals, the initial mechanism of frazil nucleation is not completely understood. The available data seems to support that the formation of frazil is started by the introduction of seed crystals into supercooled water. The concept of mass exchange at the air/water interface proposed by Osterkamp (64) is the most probable mechanism by which the seed crystals are introduced. The origin of the seed crystals and

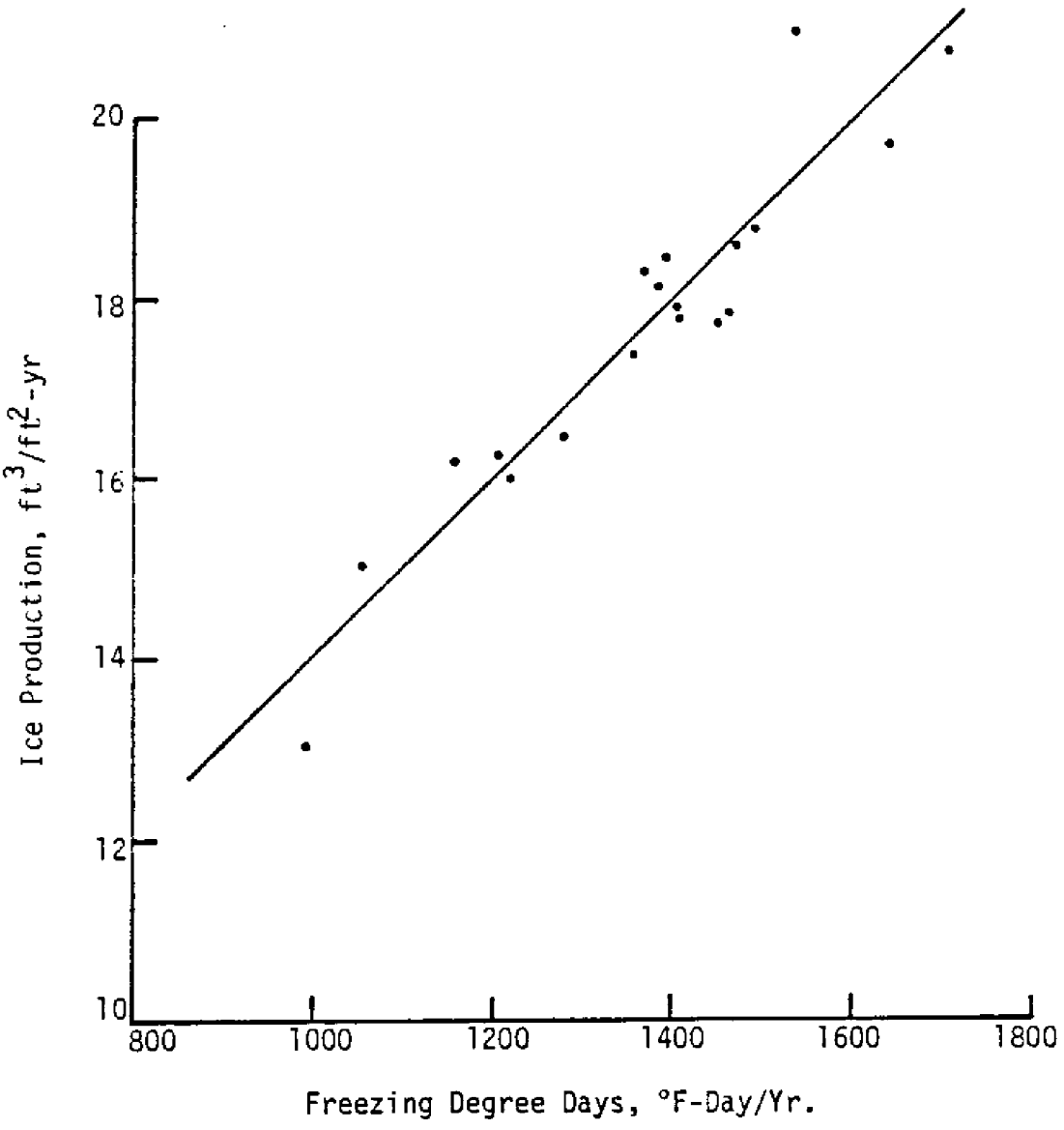

Figure 6. Correlation between seasonal values of ice production and air temperature, St. Lawrence River at Massena, N.Y. (78).

the rate at which they are introduced will depend on the local environmental conditions. Water originating in a river and then introduced into the air by bubble bursting, splashing, windspray, evaporation, etc., can freeze and return to the river in the form of seed crystals to initiate the formation of frazil ice in rivers. It is interesting to note that minimum air temperatures of -9 to -8^{o}C are often reported as necessary for the production of frazil. These temperatures correspond to the minimum temperatures at which spontaneous heterogeneous nucleation could be expected in water particles suspended in air. Ice particles that originated at some distances above the water body, such as snow, frost, ice particles from trees, shrubs, etc., could be effective seed crystals. Very cold soil particles and cold organic materials at temperatures less than the supercooling level necessary to cause spontaneous nucleation can also be introduced across the air/water interface and may serve to nucleate ice, although their effectiveness is not known.

The mass exchange mechanism provides a reasonable explanation for the observation of ice crystals at the water surface at the start of frazil formation. This mechanism cannot explain the existence of all frazil crystals, however. The number of ice crystals increases rapidly when a crystal is introduced into turbulent supercooled water in which spontaneous nucleation is not possible. This increase in the number of crystals occurs only because of the presence of the original seed crystal and secondary nucleation. Therefore, to determine the rate of increase of frazil ice crystals, the rate of

introduction of new crystals and the rate of secondary nucleation must be known. The relative magnitude of these rates will depend on the local environment; however, the rate of secondary nucleation is probably much greater than the rate of introduction.

In regions with very low velocity, frazil ice crystals formed at the surface of the water freeze together and rapidly grow into a thin cover which thickens during the winter. In fast flowing channels, the turbulent mixing will both supercool the water over the entire depth and entrain frazil crystals deep into the flow to prevent the formation of the thin static ice cover (55). Active frazil ice adheres to river bottom material and leads to the formation of anchor ice (2). The suspended frazil ice will agglomerate and eventually float to the surface to form a moving surface layer of ice pans, floes and slush ice mixture. This moving surface layer may develop into a continuous ice cover initiated by the formation of an ice bridge or surface ice jam at a river section or from an artificial obstacle.

In rivers with fast flow velocity or steep gradient, a natural stable ice cover will not form. Without the existence of an ice cover the production of frazil ice will continue in order to balance the surface heat loss. Once formed, the frazil ice will sweep underneath a downstream ice cover and eventually accumulate on the underside of the cover. Massive undercover accumulations of ice mass, termed hanging dams, have been found in both large and small rivers (14,49,60,83,84). The hanging dams can block the water passage and lead to substantial changes

in water levels. The large accumulation of frazil ice in the river may eventually lead to extensive flooding by forming ice jams in the spring (36).

Growth and Decay of Ice Cover

The thermal growth and melting of the ice cover can take place on both the air-ice and the ice-water interfaces, Fig. 7. The growth and decay of the ice cover is governed by the heat conduction across the thickness of the ice cover, which can be described as

$$\rho_i C_i \frac{\partial T}{\partial t} = \frac{\partial}{\partial z} \left(k \frac{\partial T}{\partial t}\right) + \phi_p(z,t) \qquad (33)$$

in which ρ_i = density of ice, 0.92 g/cm^3; C_i = specific heat of ice, 1.0 cal g^{-1} $^oC^{-1}$; k = thermal conductivity of ice, 0.0053 cal cm^{-1} s^{-1} $^oC^{-1}$; ϕ_p = rate of internal heating per unit volume due to the adsorption of shortwave penetration, Eq. 5; T = temperature in the ice cover, in degrees Celsius; and z,t = space and time variables, respectively.

The ice surface is assumed to be well-drained during the melting period. As a consequence, the growth of the ice cover is assumed to take place only at the ice-water interface. These assumptions can be justified by considering the existence of cracks in the ice cover for drainage and furthermore that no flooding of river water can occur over a floating ice cover (106). At the upper boundary, the boundary condition is

$$k \frac{\partial T}{\partial z} = \Sigma \phi_i - \rho_i L_i \frac{d\theta}{dt} \quad ; \quad \text{at } z = 0 \qquad (34)$$

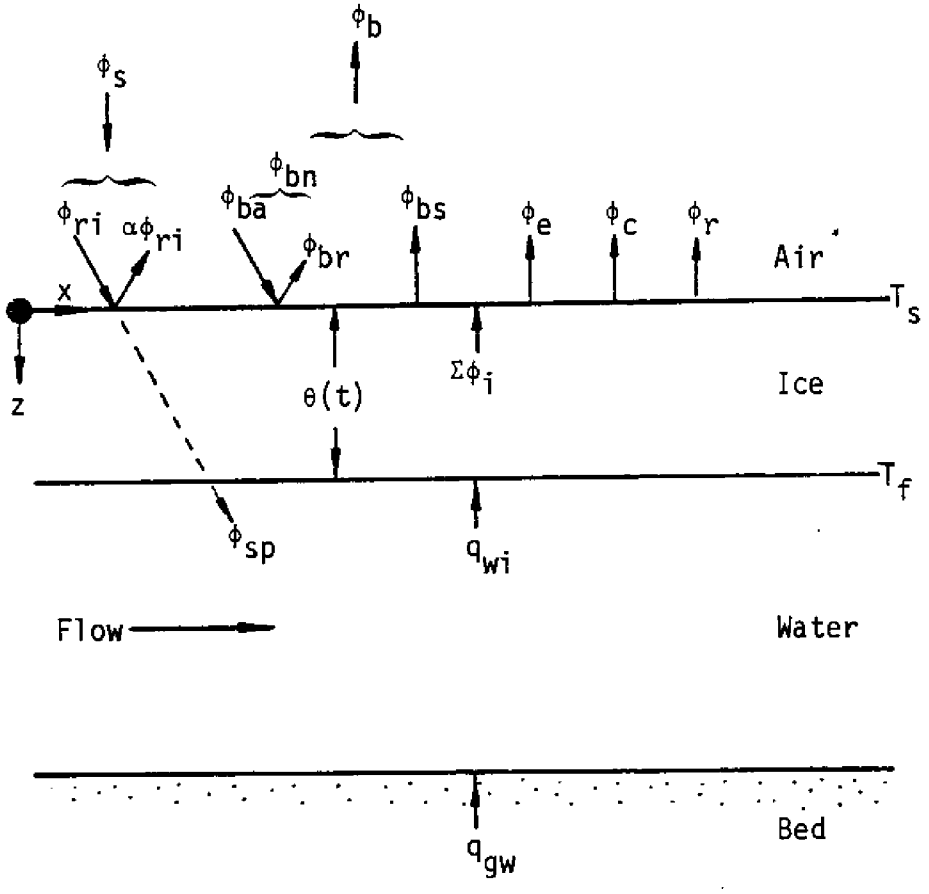

Figure 7. Heat exchanges in a river ice cover (88).

in which $\Sigma\phi_i$ = net heat loss rate at the air-ice interface excluding ϕ_s; θ = thickness of the ice cover, in centimeters. Similarly, the boundary condition at the lower boundary is

$$k \frac{\partial T}{\partial z} = q_{wi} + \rho_i L_i \frac{d\theta}{dt} \quad ; \quad \text{at } z = \theta \tag{35}$$

in which q_{wi} = net flux from water to the ice cover. The heat flux q_{wi} is a function of local water temperature T_w, which can be determined from Eq. 27. The boundary value problem defined by Eqs. 33-35 is a nonlinear problem, which can be solved by finite-difference techniques (43,44). However, the time-dependent ice growth and decay at each station along the river can be approximated by a one-dimensional, quasi-steady state linear temperature distribution over the thickness of the ice cover. [The validity of linear temperature distribution for thin ice covers has been examined by Greene (44).] For the quasi-steady state linear temperature distribution, Eq. 33 can be approximated at each time step by

$$\frac{\partial T}{\partial z} = \frac{T_f - T_s}{\theta} \tag{36}$$

With this approximation, the shortwave contribution should be included in the heat loss term $\Sigma\phi_i$ in the boundary condition, Eq. 34. A detailed numerical model for coupled water temperature and ice thickness distributions exists (88). For practical applications a simple stepwise integration procedure can be used (7,80). In this procedure $\Sigma\phi_i$ can be expressed in

terms of a heat transfer coefficient, $\Sigma\phi_i = h_{ia}(T_s - T_a)$. The ice surface temperature can then be calculated by

$$T_s = \frac{kT_f + T_a h_{ia}\theta}{h_{ia}\theta + k} \tag{37}$$

If the calculated $T_s < T_f$, then the rate of change of ice cover thickness is

$$\rho_i L_i \frac{d\theta}{dt} = \frac{k(T_f - T_s)}{\theta} - h_{wi}(T_w - T_f) \tag{38}$$

If the calculated $T_s > T_f$, then the top surface of the ice cover is melting. The surface temperature is T_f and

$$\rho_i L_i \frac{d\theta}{dt} = - h_{ia}(T_a - T_f) - h_{wi}(T_w - T_f) \tag{39}$$

in which, T_s = temperature on the top surface of the cover; T_a = air temperature; T_f = melting point, 0^oC; k = thermal conductivity of ice; θ = ice cover thickness; h_{ia}, h_{wi} = heat transfer coefficients at the air-ice and ice-water interfaces. Eqs. 38 and 39 can be used to determine the ice cover thickness through stepwise integrations. The water temperature can be efficiently calculated using a Lagrangian finite-difference solution of Eq. 27 with $\Sigma\phi_i$ as the heat exchange term (7). In the preceding discussion, effects of snow cover above the ice sheet and the accumulation of frazil ice were not considered. Both of these can influence the heat exchange through the ice cover. These heat exchange effects can be accounted for by

adding appropriate layers to the ice cover (8,9). The frazil accumulation tends to accelerate the thickness growth since less water mass is required to be frozen in the frazil layer (23). The snow cover generally tends to retard the growth in ice thickness through its insulation effect. In regions with heavy snow fall, however, the submerged portion of the thick snow accumulation on the ice cover can lead to the formation of snow ice and compensate for the insulation effect on ice thickness growth.

Further simplifications can lead to an empirical degree-day model (86).

$$\theta = (h_i^2 + \alpha S)^{1/2} - \beta D_t^{\gamma} \qquad (40)$$

in which, h_i = initial ice cover thickness; D_t = number of days since the formation of the ice cover, S = cumulative degree-days of freezing since the formation of the ice cover; α = an empirical coefficient which is a constant during the growth period and decreases linearly with the air temperature during the decay period; β and γ = empirical constants which account for the suppression effect of the turbulent heat flux from the river water. The value of γ is approximately 1.0.

Assuming that the turbulent heat transfer q_{wi} is equal to zero, $T_s = T_a$, and the initial thickness h_i is negligible, Eq. 40 reduces to the classical degree-day formula for ice thickness growth.

$$\theta = \alpha_o S^{1/2} \quad (41)$$

Theoretically, the value of α_o is 1.0 $day^{-1/2}$ $^oF^{-1/2}$ for ice covers free of snow. This value is much higher than the acutal values due to the assumptions introduced. Empirical values of α_o are given in Table 3. Eq. 41 is applicable only to the growth period, Bilello (19) suggested the use of an accumulated thawing degree-days formula to describe the decay and breakup of ice cover from their maximum thicknesses.

$$\theta = \theta_{max} - \alpha'_o S_T \quad (42)$$

in which, θ_{max} = maximum ice thickness at the beginning of the ice decay; S_T = accumulated thawing degree-days, and α'_o = an empirical constant that is site dependent.

Table 3. Typical values of coefficient α_o (56)

Ice cover condition	α_o (in. $^oF^{-1/2}$ $day^{-1/2}$)	α_o (cm $^oC^{-1/2}$ $day^{-1/2}$)
Windy lakes with no snow	0.8	2.7
Average lake with snow	0.5~0.7	1.7~2.4
Average river with snow	0.4~0.5	1.3~1.7
Sheltered small river with rapid flow	0.2~0.4	0.7~1.4

IV. ICE ACCUMULATION AND TRANSPORT

At the beginning of the winter as the ice is being produced and transported along the river, a significant portion of it will rise to the surface to form a moving layer of a mixture of ice floes, pans, and slush. The concentration of this surface layer increases as it moves downstream. The downstream transport of the surface ice will cease when it reaches an artificial obstacle or a river section where an ice bridge across the river is formed by the congestion of the ice. Once an obstacle is reached the incoming surface ice will accumulate at its upstream side and extend the ice cover upstream. Frazil ice that remains in the suspension underneath the surface layer will be transported downstream and deposited on the underside of the ice cover to form a layer of frazil ice accumulation.

The phenomena of ice bridging is not well understood, even though ice bridges usually form at the same location of a river each winter. The formation of an ice bridge at a river section is related to the ice transport capacity of the section and the rate of ice discharge coming from upstream. The maximum rate of ice discharges that can pass through a river while not forming an ice bridge is dependent on the flow velocity, channel top width between banks or border ice boundaries, surface slope, size and concentration of ice in the surface layer (1,26).

The upstream progression of ice cover from an obstacle is dependent on the rate of ice supply from upstream and the river flow conditions. In low velocity reaches, a relatively thin smooth cover can be formed while in other reaches ice jams or

hanging dams may form before upstream progression can proceed. The above discussion is presented in the context of ice cover formation in the beginning of the winter. A similar process can occur when a large volume of surface ice floes is released during the breakup of ice cover upstream. In this case, the leading edge of the intact downstream ice cover often acts as the obstacle which initiates the ice accumulation process.

Ice Cover Progression

Once an ice cover is initiated, it will progress upstream through the accumulation of incoming surface ice floes and slush. The rate of progression of the leading edge of an ice cover, V_{cp}, can be calculated from the conservation of mass

$$V_{cp} = (1 + \frac{V_{cp}}{V_s}) \ (\frac{Q_i^s}{1-e}) / [h_i (1-e_p) B_c] \qquad (43)$$

in which, Q_i^s = surface ice discharge; h_i = thickness of the ice cover formed by the accumulation; e = porosity of individual ice floes; e_p = porosity in the accumulation between ice floes; B_c = width of the newly accumulated cover; and V_s = mean velocity of the incoming surface ice discharge.

In order for an ice cover to progress, a stability condition for incoming ice floes must be satisfied. The stability of an ice floe, when the leading edge thickness of the ice cover equals that of the ice floe, can be determined by an equilibrium analysis of an arriving ice floe (4,35,103). Using a "no-spill" condition, the stability criteria was shown to be (4)

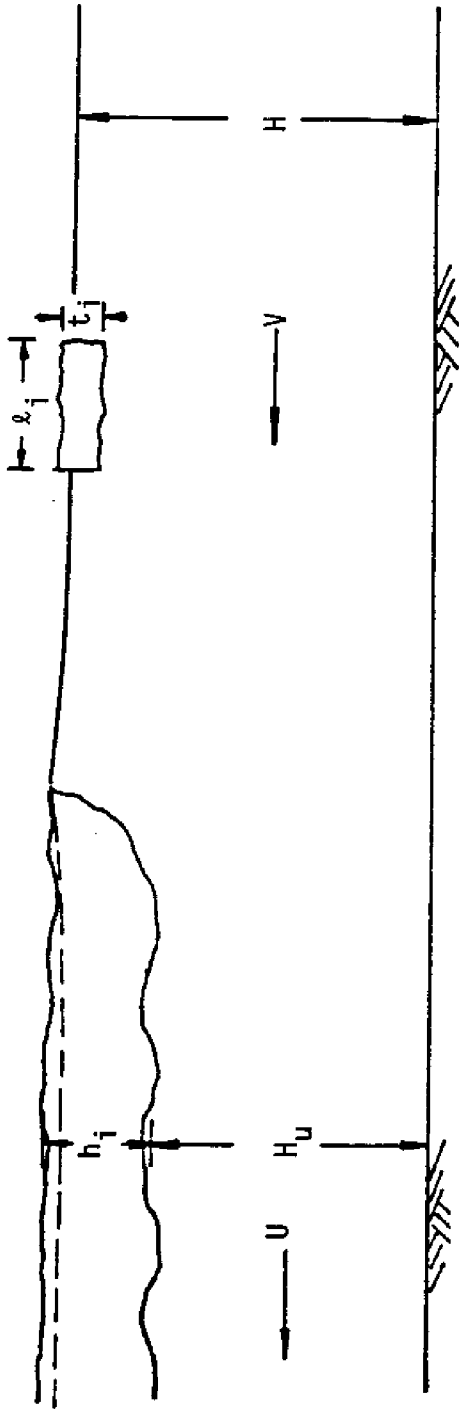

Figure 8. Definition sketch for ice cover progression.

$$\frac{V_c}{[gt_i(1-\frac{\rho_i}{\rho})]^{1/2}} = \frac{2(1-\frac{t_i}{H})}{[5-3(1-\frac{t_i}{H})^2]^{1/2}} \quad (44)$$

in which, V_c = critical velocity upstream of leading edge for underturning and submergence; t_i = thickness of the ice floe; H = upstream flow depth; and g = acceleration of gravity. A similar expression has been obtained by Pariset and Hausser (66,67).

$$F_{rc} \equiv \frac{V_c}{\sqrt{gH}} = F(\frac{t_i}{\ell_i})\ (1-\frac{t_i}{H})\sqrt{2(\frac{\rho-\rho_i}{\rho})(1-e)\ \frac{t_i}{H}} \quad (45)$$

where, $F(t_i/\ell_i)$ = a form factor which varies between 0.60 and 1.30; ℓ_i = length of the ice floe. Eqs. 44 and 45 are identical if $F(t_i/\ell_i) = \sqrt{2}/[5-3(1-t_i/H)^2]^{1/2}$. The effect of porosity, e, of an ice floe is included in Eq. 45 (56). Under the criteria given by Eqs. 44 or 45, an ice cover of one floe thickness will form by simple juxtaposition.

At a velocity higher than V_c, incoming ice floes will submerge and deposit on the underside of the cover. This leads to a gradual increase of ice cover thickness in the vicinity of the ice front. The velocity that is required for ice floes to submerge below the ice cover increases with the thickness of the ice cover. For a given flow depth and velocity upstream of the ice front, a limiting value exists for the accumulation thickness of an ice cover during its progression. Pariset , et al. (66,67), Michel (56,57), and Tatinclaux (100) have developed methods for predicting the equilibrium thickness h_i of the ice cover formed by floe accumulation. For a given flow condition,

the thickness h_i may be estimated by (57,58)

$$\frac{V}{\sqrt{gH}} = (1- \frac{h_i}{H}) \sqrt{2(1-e_c)(1- \frac{\rho_i}{\rho}) \frac{h_i}{H}} \qquad (46)$$

From Eq. 46, one can show that there is a maximum Froude number for the flow in front of an ice cover at which it becomes unstable and can not progress further upstream. This critical Froude number, which occurs when $h_i/H = 0.33$, is

$$F^*_{rc} = \frac{V_c}{\sqrt{gH}} = 0.158 \sqrt{1-e_c} \qquad (47)$$

in which, $e_c = e_p + (1-e_p)e$, is the overall porosity of the ice accumulation. This equation indicates that e_c has an important effect on the progression of an ice cover. For $e = 0.55$ and $e_p = 0.4$, one gets $F^*_{rc} = 0.082$. Field observations (51) indicated F^*_{rc} can vary from 0.05 to 0.10 for different floe and accumulation characteristics. Newly formed ice floes will have higher porosity and, therefore, smaller F^*_{rc}. If the ice thickness resulting from Eq. 46 leads to an undercover velocity U exceeding the critical velocity of entrainment for ice floes on the underside of the cover, the ice cover thickness will then be governed by this undercover entrainment velocity. In this case the ice cover progression will cease. Laboratory flume observations indicate that at F_r close to F^*_{rc} incoming floes could be carried under the accumulated ice cover and swept along the underside of the cover (98). This leads to a possible physical interpretation of the existence of F^*_{rc}. Detailed

discussion of the critical velocity for undercover entrainment will be given later in relation to the formation of hanging dams.

Ice cover thickness formulas derived from the consideration of hydraulic accumulation are often categorized as "narrow river jam" theories (66,67). This type of formulation can be used to determine the ice cover thickness if the internal resistance of the ice accumulation is able to withstand the streamwise force. For accumulations of loose ice floes or slush ice, local packing of an ice cover at its front is often observed (51). Michel (59) derived an expression for ice thickness by considering the frontal packing due to hydrodynamic thrust at the ice front.

$$\frac{U}{\sqrt{gh_i}} = \left[\frac{\cos\phi\left(\frac{\rho-\rho_i}{\rho}\right)\frac{\rho_i}{\rho}(1-e_c)\frac{h_i}{H}}{k_\ell + (1-\frac{H_u}{H})^2}\right]^{1/2} \qquad (48)$$

in which, k_ℓ = minor loss coefficient for the ice cover front; ϕ = angle of friction of granular ice mass.

A graphical summary of formulas for calculating ice cover thickness by accumulation, h_i, is presented in Fig. 9. The Froude number upstream of the leading edge, $V/\sqrt{gH}$, is used as the vertical coordinate for the convenience of interpretation.

Mechanical Thickening of Ice Cover

In a wide river the increase in streamwise force may exceed the increase in bank resistance. In this case the internal resistance of the ice accumulation will be unable to resist the increasing streamwise force as the cover progresses upstream. If the stress in the ice accumulation exceeds its internal strength, the cover will collapse and thicken until an

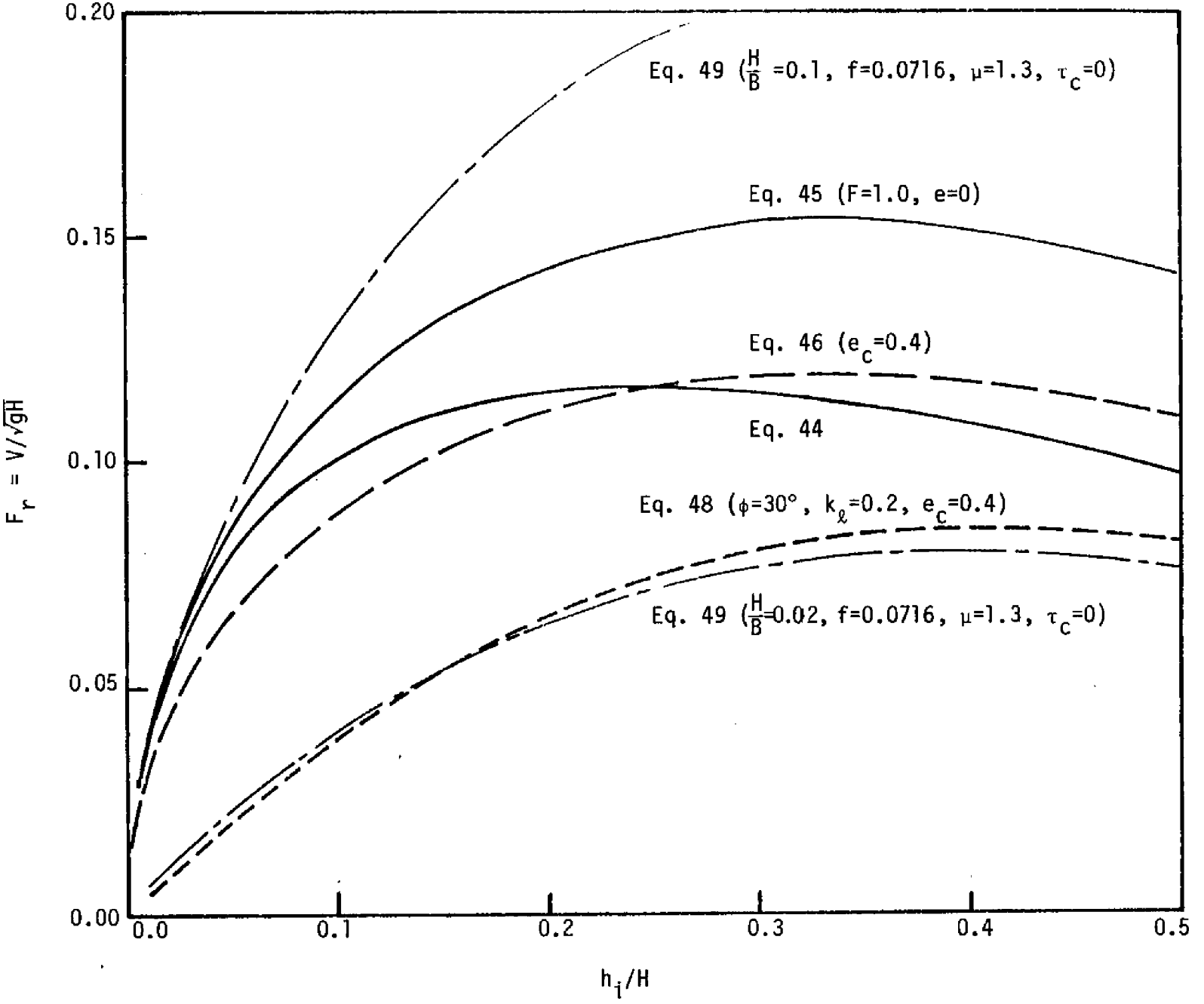

Figure 9. Relationship between Froude number and the ice accumulation thickness.

equilibrium thickness is reached (58,66,104). This process of mechanical thickening is commonly known as "shoving", and an accumulation of this kind is often called "wide river jams" (66,67). When shoving occurs, a relatively long reach of ice cover will suddenly collapse and the leading edge will move a long distance downstream. Based on the analysis of Pariset and Hausser (66,67) and Uzuner and Kennedy (104), the following equation for the equilibrium thickness h_i can be obtained for steady uniform flows.

$$\left[f_i + \frac{\rho_i}{\rho}\,(f_b+f_i)\,\frac{h_i}{d_w}\right]\frac{U^2B}{8g} = \frac{2\tau_c h_i}{\rho g} + \mu(1-e_p)\left(1-\frac{\rho_i}{\rho}\right)\frac{\rho_i h_i^2}{\rho} \qquad (49)$$

in which, f_i and f_b = Darcy-Weisbach friction factors related to the ice covers and the channel bed, respectively; d_w = depth of flow under the ice cover. Bank resistance per unit length of the ice cover is quantified as $\tau_c h_i + \mu F_s$, where $\tau_c h_i$ is the cohesive contribution; μF_s is the ice-over-ice friction term; and F_s is the streamwise force per unit width of the cover. The coefficient μ has a value of about 1.28, and $\tau_c h_i$ varies between 75 lb/ft and 91 lb/ft (67). Eq. 49 was obtained by considering the ice cover as an accumulation of granular material. A plot for Eq. 49 is included in Fig. 9 to provide a comparison between ice thickness resulting from different river conditions. Michel (59) has pointed out that it takes only a little freezing to form a solid crust on the top of the ice cover and prevent the occurrence of shoving.

Hanging Ice Dams and Undercover Transport

Large accumulations of ice mass in rivers is commonly known as hanging dams. According to their formation processes, hanging dams may be classified into two categories (83,84). The first type of hanging dams, which will be referred to as surface ice hanging dams, are accumulations of surface ice floes or frazil ice pans, formed near the leading edge of an ice cover during its upstream progression. The initial thickness of the ice cover formed during the leading edge progression can be estimated by Eqs. 46 or 48 using the local value of $V/\sqrt{gH}$. Since the depth and velocity varies along (and across) the river, the initial thickness of the ice cover in a river will not be uniform. In fast flowing regions, the initial ice cover will appear as large localized ice accumulations in the form of hanging dams. When the ice cover leading edge reaches a rapid section with an upstream Froude number exceeding F^*_{rc}, incoming surface ice pans and slush will be forced to pass underneath the cover and carried downstream until the velocity of the flow becomes low enough for them to deposit. These depositions will then increase the thickness of the existing ice cover and hanging dams. Mechanical thickening can occur during the above described process when the shoving condition given by Eq. 49 is satisfied.

Little is known about the mechanism of the transport and accumulation of ice floes on the underside of the ice cover. Using laboratory data by Filippov (39), Ashton (5) obtained empirical relationships, as shown in Fig. 10, for the undercover travel distance of ice floes

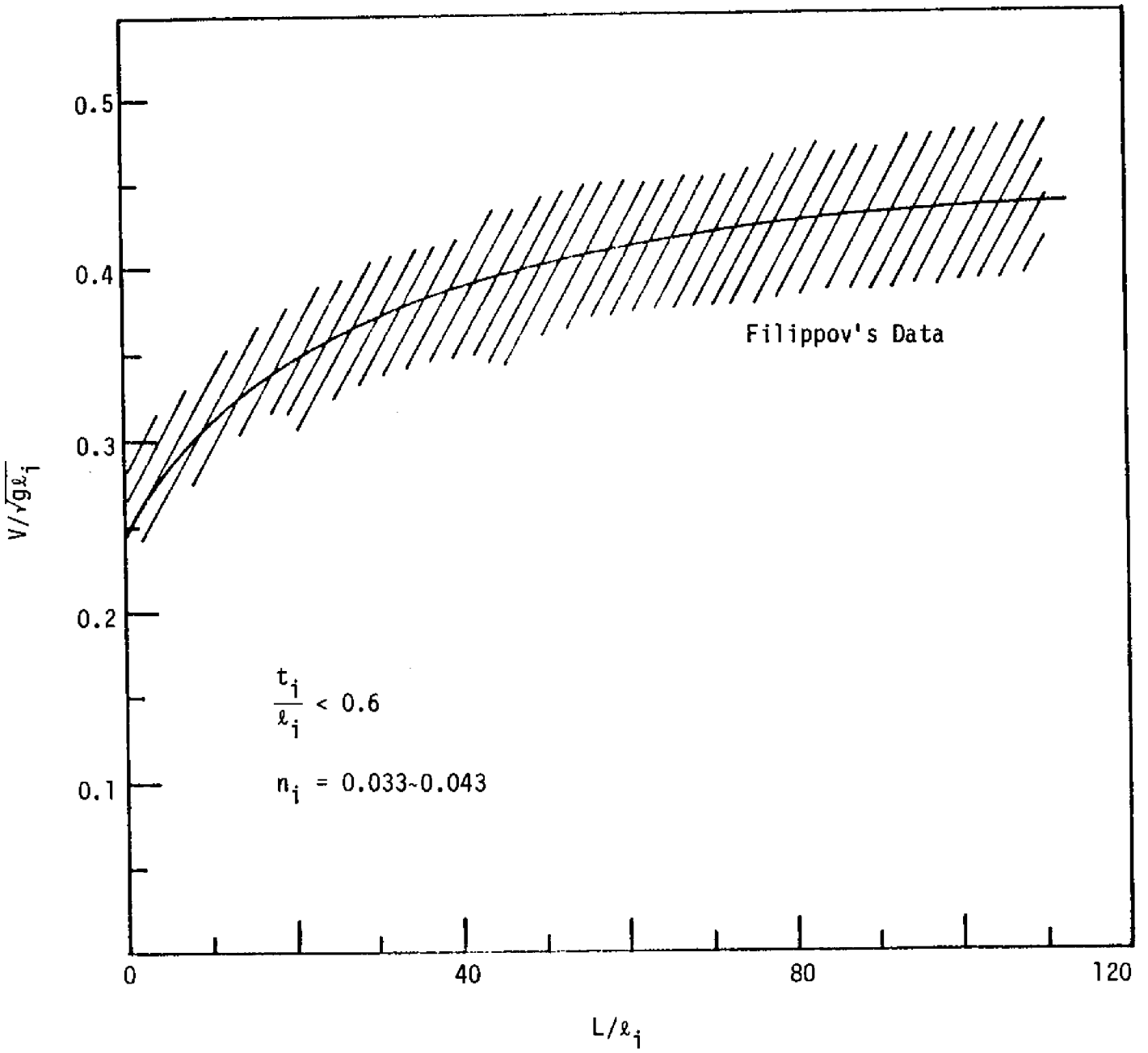

Figure 10. Transport distance (L) for ice floes.

$$\frac{L}{\ell_i} = f\left(\frac{V}{\left[g\cdot\frac{\Delta\rho}{\rho}\cdot\ell_i\right]^{1/2}}\ ,\ \ n_i\ \ ,\ \ \frac{t_i}{\ell_i}\right) \tag{50}$$

in which, L = undercover travel distance of an ice floe before its rest; V = mean velocity upstream of the cover; $\Delta\rho = \rho - \rho_i$; n_i = Manning's roughness coefficient of the underside of the ice cover, and ℓ_i = length of the block. The experimental data indicate that when t_i/ℓ_i decreases or n_i increases the value of L/ℓ_i decreases. Tatinclaux and Gogus (99) studied the re-entrainment criteria of an ice floe resting under the ice cover behind an artificial obstacle of height δ equal to or less than t_i. Based on laboratory data, they found that the critical Froude number for entrainment can be expressed in terms of the ratio t_i/ℓ_i and size of the obstacle δ

$$F_e \equiv \frac{U}{\sqrt{g\,\frac{\Delta\rho}{\rho}\,t_i}} = \left[C_1\left(\frac{t_i}{\ell_i}\right)^2 + C_2\left(\frac{t_i}{\ell_i}\right) + C_3\right]^{-1/2} \tag{51}$$

where C_1, C_2, and C_3 = coefficients which are dependent on the size of the obstacle. Suggested values for C_1, C_2 and C_3 are -2.26, 2.14 and 0.015, respectively, for $\delta = 0$. Both Eqs. 50 and 51 are applicable to a flat ice cover.

The second type of hanging dams, which will be referred to as frazil ice hanging dams, are formed by the deposition of suspended frazil ice particles on the underside of a stable ice cover. These frazil ice particles are produced in open water areas upstream of a stable ice cover during periods of supercooling. In the early stages of their production, frazil particles are active, which means that they very readily stick to any surface with which they come into contact. Therefore,

near the leading edge of a river's ice cover, almost all of the frazil particles that reach the ice-water interface are deposited. Frazil particles, which remain entrained in the flow, lose some of their adhesiveness and become inactive. Therefore, further downstream from the leading edge, these frazil particles will deposit on the underside of the ice cover only in regions of relatively low flow velocity. Based on observations in the LaGrande River, Michel and Drouin (61) suggested that the critical velocity for ice deposition ranges between 0.6 and 1.3 m/sec. Shen and VanDeValk (83) found that this critical velocity is about 3 ft/sec in the upper St. Lawrence River. Besides the activeness of the frazil ice, the rate of deposition is depended upon the buoyant velocity and the concentration of the frazil ice suspension (45). Neither the buoyant characteristics nor the adhesive properties of frazil ice particles are well understood.

For a surface ice hanging dam, which is located near the leading edge of an ice cover, a relatively soft outer layer of frazil slush could form on the surface due to the accumulation of active frazil ice particles produced in the open water area during the winter. Such hanging dams have been found in the St. Lawrence River (83,84).

Simulation of Ice Cover Formation

A few computer models exist for simulating flow and ice conditions in a river (25,61,70,71,72,89,94). Ice cover formation is a major component in these models. In applying the existing theories to a natural river, it is important to recognize that the flow conditions in the river are continuously

changing in space as well as in time. During the ice formation period, the progression and thickening of the ice cover can cause a rapid change in a river's flow conditions especially in steep shallow rivers. The processes and evolution of the initial ice cover as discussed in this chapter can be summarized as in Figure 11. Figure 11 is developed for one-dimensional models. Two-dimensional effects, which appear to be very important for the distribution of ice cover thickness and the progression of ice fronts in large rivers, are presently being studied (48).

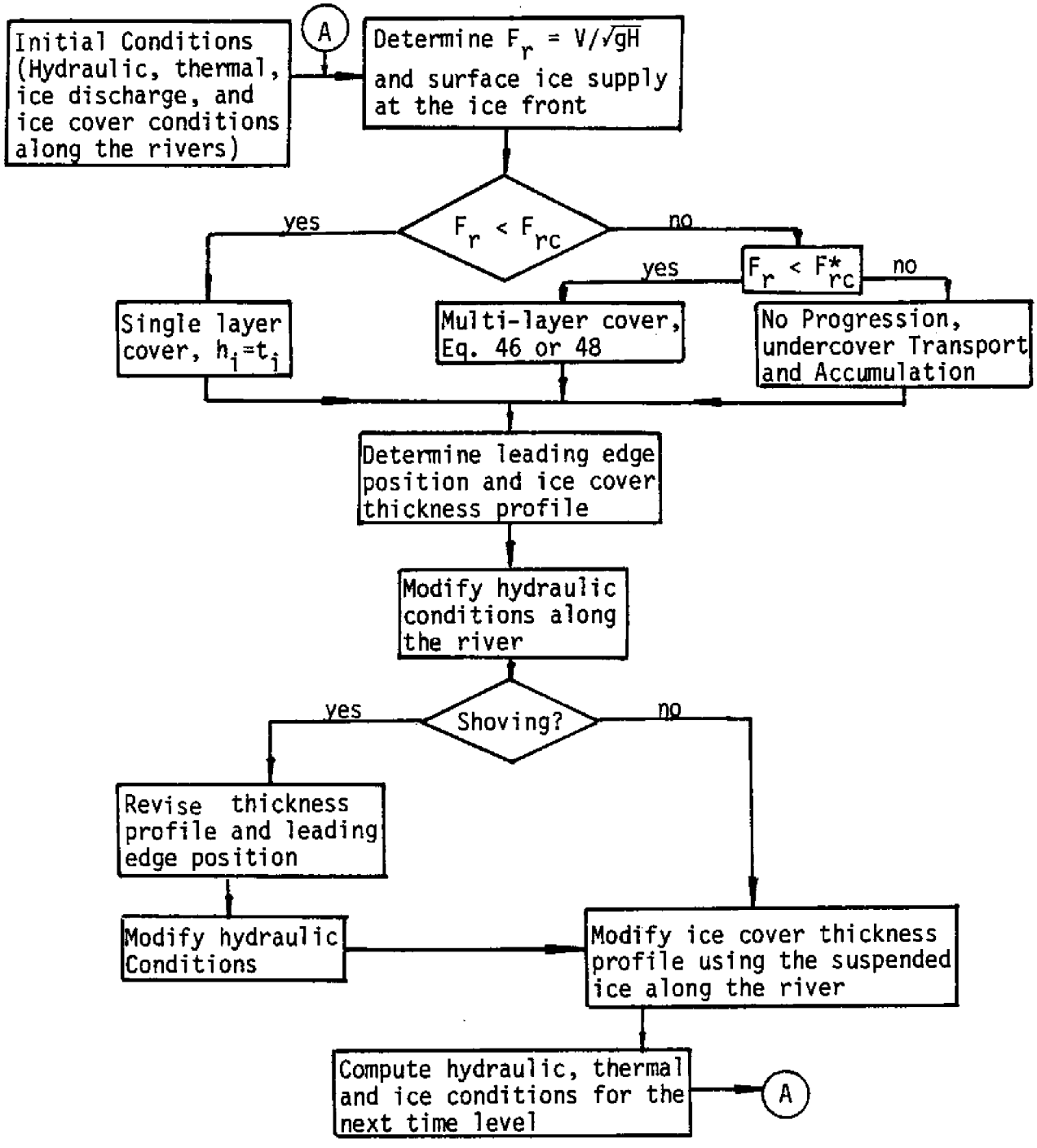

Figure 11. Ice Cover Formation Processes

V. HYDRAULICS OF ICE-COVERED RIVERS

The flow condition in a river not only influences but also interacts with its ice condition. Except in very narrow channels, the ice cover is able to accommodate gradual changes in water level and can be considered as floating in hydrostatic equilibrium. Stage and discharge variations of a gradually varied flow in a river with floating ice covers can be described by the continuity equation

$$\frac{\partial Q}{\partial x} + \frac{\partial A}{\partial t} = 0 \tag{52}$$

and the momentum equation

$$\rho \frac{\partial Q}{\partial t} + \rho\left[\frac{2Q}{A}\frac{\partial Q}{\partial x} - \frac{Q^2}{A^2}\frac{\partial A}{\partial x}\right] + \rho g A \frac{\partial H_e}{\partial x} + (p_i\tau_i + p_b\tau_b) = 0 \tag{53}$$

in which, Q = discharge; A = flow area; $H_e = z_b + d_w + \bar{h}_i$, water level; z_b = bed elevation; d_w = depth of flow; $\bar{h}_i$ = equivalent thickness of the ice cover, $\rho_i\theta/\rho$; p_b, p_i = wetted perimeter formed by the channel bed and the ice cover, respectively; τ_b, τ_i = shear stress at the channel bottom and at the ice-water interface, respectively.

To solve Eqs. 52 and 53 for Q and H_e, it is necessary to know the geometry of the cover and the additional resistance induced by the ice cover. The estimation of the ice cover geometry including its thickness and areal extent may be obtained according to information discussed in previous chapters. The resistance term in Eq. 53 can be expressed in

terms of the resistance coefficients of the underside of the ice cover and the channel bed.

Roughness Parameters

In river hydraulics, the friction term in Eq. 53 is often expressed in terms of the frictional slope, S_f.

$$S_f = (p_i\tau_i + p_b\tau_b)/(\rho g A) \tag{54}$$

This boundary resistance is usually measured in terms of the Chezy C, the Darcy-Weisbach f, or the Manning n. For uniform flow these three parameters can be related by Eq. 55.

$$\frac{C}{\sqrt{g}} = \frac{(1.486)}{\sqrt{g}} \frac{R^{1/6}}{n} = \left(\frac{8}{f}\right)^{1/2} \tag{55}$$

in which R = hydraulic radius. The friction factor f is dimensionless and has the most general range of application. However, it has the drawback of being a function of the Reynolds number and relative roughness both of which are a linear function of R. Chezy's C has the disadvantage of being dimensional and varying significantly with flow. Manning's n, although dimensional and only applicable to fully rough flows, is nearly constant over a wide range of R for a given roughness height. Hence, it has been used for the analysis of most river flows (32,77).

Uzuner (102) and Pratte (75) reviewed different methods of calculating the roughness coefficient for ice-covered channels and showed that the method of Larsen (53) is the most rigorous. By dividing the flow depth into two zones at the maximum

velocity plane, assuming zero shear stress at this plane, and using the Karman-Prandtl velocity formula for both zones, Larsen showed that the equivalent Manning coefficient, n_c, of an ice-covered channel can be calculated by Eq. 60.

$$\frac{1}{n_c} = \frac{\frac{1}{n_i} d_i^{5/3} + \frac{1}{n_b} d_b^{5/3}}{(\frac{1}{2})^{2/3} d_w^{5/3}} \tag{60}$$

in which, n_c = equivalent Manning's coefficient; n_i and n_b = Manning's coefficients of the ice cover and the channel bed; d_w = total flow depth; d_i and d_b = depths of flow above and below the maximum velocity line. The depth ratio d_i/d_b can be expressed as:

$$d_i/d_b = [\frac{a\ (b-1)\ n_i}{b\ (a-1)\ n_b}]^{3/2} \tag{61}$$

in which, $a = \ln(30\ d_b/k_b)$; and $b = \ln(30\ d_i/k_i)$. For channels with small relative roughnesses, Eq. 60 can be simplified to the Belokon-Sabaneev formula (62,102).

$$n_c = [\frac{1}{2}\ (n_i^{3/2} + n_b^{3/2})]^{2/3} \tag{62}$$

Larsen suggested two methods for determining the roughness height from a measured vertical velocity profile. In the first method, the roughness height and Manning's coefficient of the underside of the ice cover can be determined from the measured velocity profile above the plane of the maximum velocity by using Eq. 63.

$$k_i = 30\ y\ \exp[-1/(1-\bar{v}/v)] \quad ; \quad n_i = 0.032\ k_i^{1/6} \tag{63}$$

in which, v = velocity at depth y below the ice-water interface; $\bar{v}$ = mean velocity between the ice-water interface and the depth y; k_i = roughness height of the ice cover. In the second method, the velocity profile is first obtained by fitting the measured velocity data by a straight line on a semilogarithmic plot. The roughness height is then determined from the fitted velocity profile. This second method is the least desirable of the two methods due to difficulties involved in determining a best-fit line from the measured data. Some of these difficulties are discussed by Calkins, et al. (27).

It should be pointed out that, since Larsen's formulation was derived for a channel with a flat ice cover, this formulation is not valid for locations with large localized accumulations of ice, such as hanging ice dams.

Tatinclux and Gogus (100) discussed the deficiency of assuming zero shear stress at the maximum velocity plane, and suggested a refined method for analyzing flow in channels with large differences between the ice cover and channel bed roughness.

The Manning equation can be derived based on the "1/6 power law" approximation of the logrithmic velocity profile for free surface flow in a wide rectangular channel with rough walls (93)

$$\frac{v}{v_*} = 5.75\ \ln\frac{R}{k} + 6.25 \tag{64}$$

For R/k less than 5 the "1/6 power law" is a very poor approximation of Eq. 64. Gerard, et al. (40,41,42) suggested the use of average roughness height to quantify the boundary resistance. In terms of roughness heights, the Belokon-Sabaneev formula becomes

$$k_t = [\frac{1}{2} (k_i^p + k_b^p)]^{1/p} \; ; \; p = \frac{2m}{2m+1} \tag{65}$$

in which, k_t = the composite roughness; k_i and k_b = the effective ice cover and bed roughness, respectively; and m = exponent of the appropriate power law.

Resistance Due to Ice Cover

The method of analysis described above can be used to evaluate local roughness coefficients from measured velocity profiles. It is not adequate, however, for the purpose of computing backwater profiles or unsteady flow modeling where the gross effect of the ice cover on the flow resistance of a river reach is required. Determination of the resistance coefficient for a river reach from recorded discharge and water level data can be made through the use of flow equations.

For steady-state flow, Eq. 53 can be written as

$$\frac{\partial H_e}{\partial x} = \frac{1}{gA} [\frac{Q^2}{A^2} \frac{\partial A}{\partial x} - \frac{1}{\rho} (p_i \tau_i + p_b \tau_b)] \tag{66}$$

in which, H_e = water level = $z_b + d_w + \bar{h}_i$. For a partially ice-covered channel, shown in Fig. 12, the resistance term can be expressed as (79):

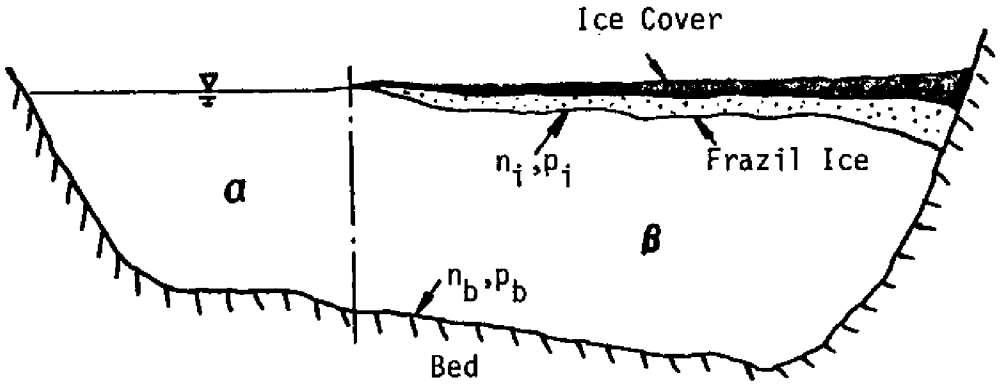

Figure 12. Flow cross-section of partially covered channel.

$$p_i\tau_i + p_b\tau_b = \gamma n_b^2 \left[\left(\frac{Q^2 p^{4/3}}{A^{7/3}}\right)_\alpha + (1+F')^{4/3}\left(\frac{Q^2 p_b^{4/3}}{A^{7/3}}\right)_\beta\right] \quad (67)$$

in which, $F' = (n_i/n_b)^{3/2}(p_i/p_b)_\beta$, α and β = subscripts which represent portions of flow areas under free surface and ice cover, respectively. The partial discharges Q_α and Q_β can be obtained from Eq. 12 (81).

$$\frac{Q_\alpha}{Q} = \frac{1}{2}\left[\frac{A_\alpha R_\alpha^{2/3}}{AR^{2/3}} + \left(1 - \frac{A_\beta R_\beta^{2/3}}{AR^{2/3}}\right)\right] \quad ; \quad \frac{Q_\beta}{Q} = 1 - \frac{Q_\alpha}{Q} \quad (68)$$

Since both the free surface case and the fully covered case can be considered as special cases of the partially covered condition, Eq. 67 can be used as a general formula. Terms with the subscript α reduce to zero for the fully covered condition and terms with the subscript β reduce to zero for the free surface condition. Based on Eqs. 66, 67, and 63, roughness coefficients of river reaches can be determined from recorded discharge and water levels. Computational methods were developed for both single channel or channel networks (68).

It is well recognized that the roughness of the underside of the ice cover varies over a wide range throughout the winter (29,47,101). Initially, the roughness is generally high as a result of the rough bottom surface of the new ice cover. The roughness gradually diminishes during the winter due to a gradual thickening of the ice cover and smoothing of the ice surface under the influence of the flowing water. The roughness reaches a minimum value and increases immediately before the spring break-up with the formation of relief features on the ice-water interface (3,29). The rate of change of ice cover

roughness is dependent on the nature of the ice cover, the flow characteristics, and meteorological conditions. The effect of meteorological conditions is particularly important in rivers with large open-water areas. In those rivers, variations of the thermal and ice conditions of the water are predominantly governed by the ambient atmospheric conditions. If the weather is mild, a decrease in ice cover roughness and reduction in frazil accumulation will occur. If the weather is cold, frazil ice will be produced in open-water regions. Accumulations of frazil ice underneath downstream ice covers may then occur causing rapid changes in the roughness of the ice cover and the flow cross sectional area.

Nezhikhovskiy (62) reviewed studies performed by Russian researchers for predicting Manning's roughness coefficient, n_i, on the underside of a river ice cover. In this review a method for estimating n_i was presented. This method considers the difference between the roughness characteristics of a smooth ice cover formed statically in a slow flowing river and rough ice cover formed from slush or ice floe accumulations in a fast flowing river. For smooth ice covers, Nezhikhovskiy suggested n_i values of 0.01 ~ 0.012 for the beginning of freeze-up, and 0.008 ~ 0.01 for the middle and end of winter. For rough ice covers, Nezhikovskiy's proposal takes into consideration meteorological conditions and the nature of the ice cover. Nezhikovskiy related the initial ice cover roughness coefficient, $n_{i,i}$ to the type of ice which forms the initial ice cover and its thickness, h_i, as shown in Fig. 13. The

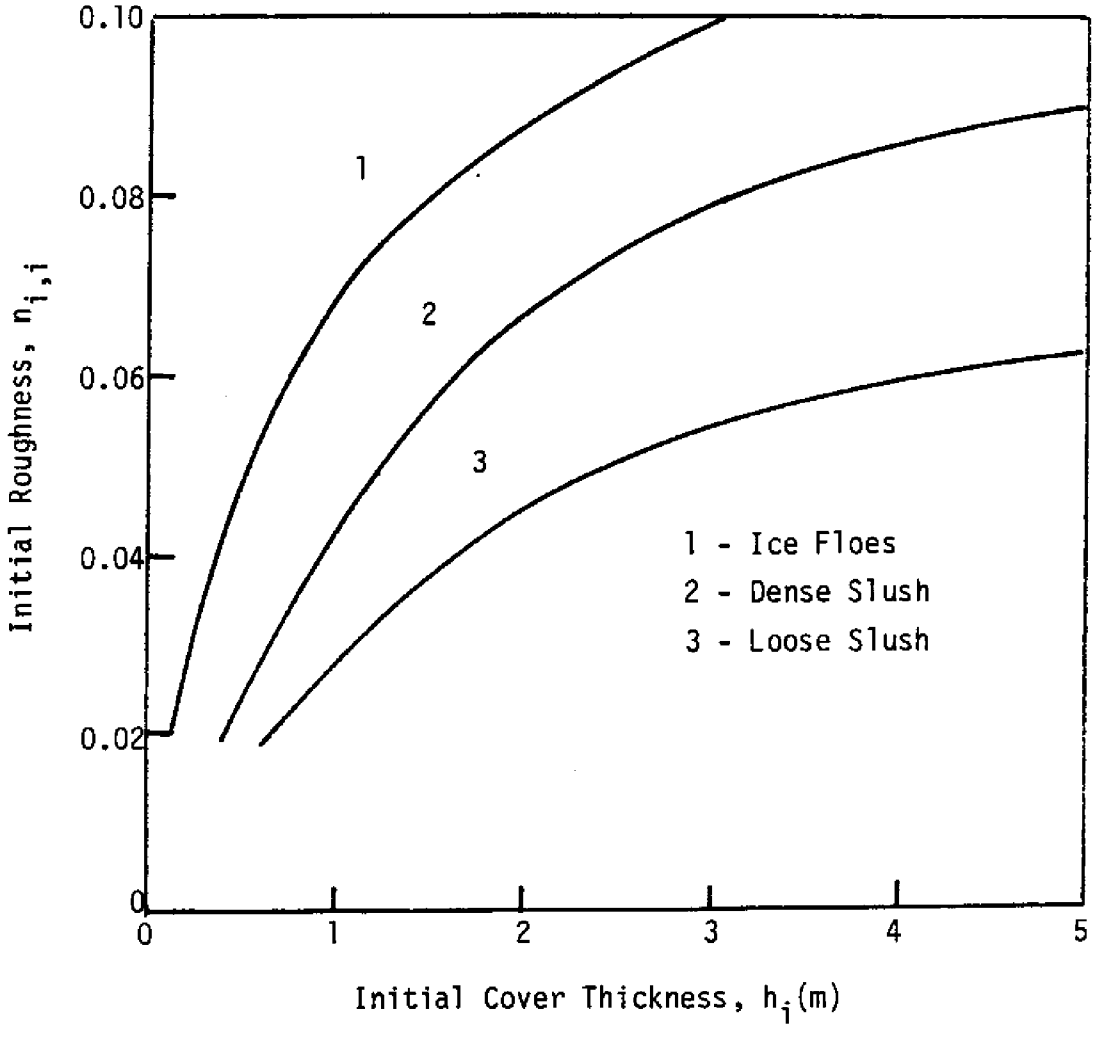

Figure 13. Relationships between the initial roughness coefficient of the ice cover and its thickness (62).

time-dependent variation of n_i during the winter is then described by the following exponential function.

$$n_i = n_{i,e} + (n_{i,i} - n_{i,e})e^{-kt} \tag{69}$$

in which, t = number of days from the beginning of the ice covered period; $n_{i,e}$ = the roughness coefficient at the end of the ice-covered period, which is found to be approximately equal to that of the smooth ice cover, 0.008 ~ 0.012; k = a decay constant which varies from river to river and year to year. Suggested values of k are given in Table 4, which show that the k value is dependent upon the severity of the winter and the relative amount of open water.

Table 4. Values of Parameter k in Eq. 69 (62)

Conditions of the Winter	Characteristics of the Ice Cover: Many Open Water Areas	Few Open Water Areas	No Open Water
Severe	0.005	0.010	0.020
Moderate	0.023	0.024	0.025
Mild	0.050	0.040	0.030

Shen and Yapa (85,108,109) analyzed data from the upper St. Lawrence River and proposed a conceptual model for the time dependent variation of the ice cover resistance coefficient. By including the effect of hanging dams, the empirical model expresses the resistance coefficient as a combination of three components, i.e. $n_i = n_d + n_t + \tilde{n}$ (Fig. 14). The first component,

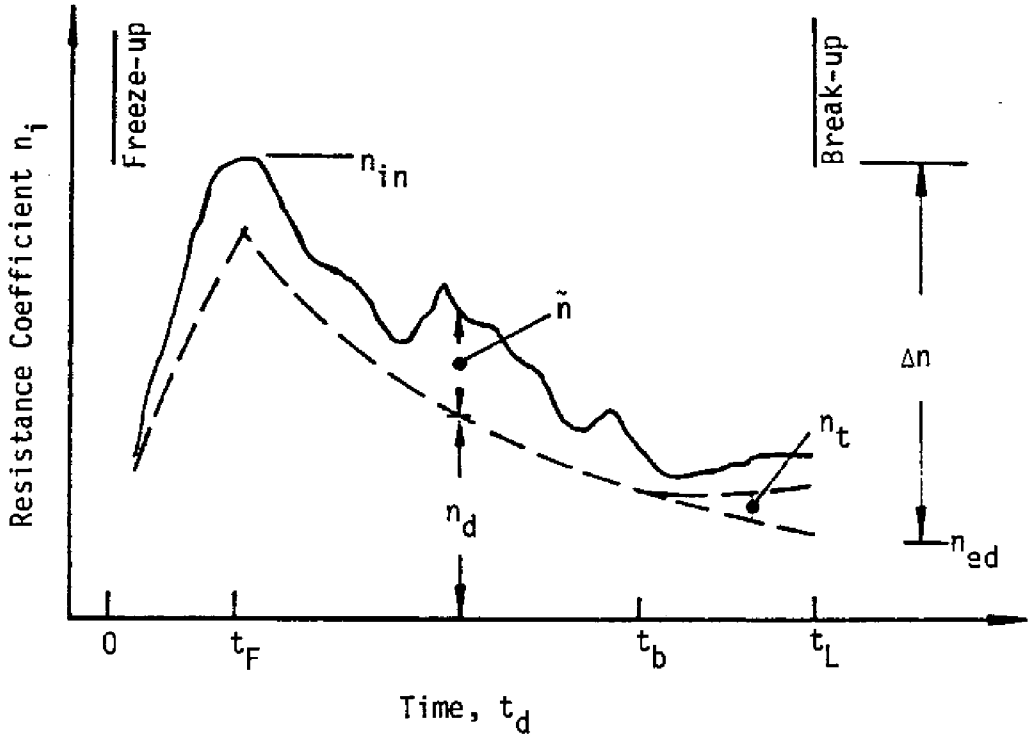

Figure 14. Seasonal variation of the resistance coefficient of ice cover.

n_d, is a simple function of time which increases monotonically during the freeze-up period and decreases monotonically during the rest of the stable ice-covered period. Expressed in functional form, the component n_d is the smaller value computed from Eqs. 70 and 71.

$$n_d = \Delta n[t/(\lambda t_F)]^{\gamma} + n_{ed} \tag{70}$$

$$n_d = \Delta n(e^{\psi t} - e^{\psi t}) + n_{ed} \tag{71}$$

where, $\psi = [1/(\delta t_L)]\log_e(\Delta n)$; t_d = time from the beginning of the freeze-up, days; t_F = duration of the freeze-up period; t_L = duration between the beginning of the freeze-up and the beginning of the break-up period; Δn = the difference between the ice roughness coefficients at the end of the freeze-up period, n_{in}, and the beginning of the breakup period, n_{ed}; λ, γ, and δ = empirical constants. Values of n_{in} and n_{ed} in a given river reach can be expressed in empirical relationships of the following forms:

$$n_{in} = f(T_{ao}, T_{wo}, A_s, AI_o, Q_o; t_i);\ t_i = t_i(T_{wo}, T_{ao}, X) \tag{72}$$

and

$$n_{ed} = a\ n_{in} + b \tag{73}$$

in which, T_{ao} = air temperature during the freeze-up period in

freezing-degree-day; T_{wo} = water temperature at the upstream end during the freeze-up period; A_s = the total surface area of the reach; AI_o = area of the ice cover at the end of the freeze-up period; Q_o = the discharge during the freeze-up period; t_i = size of the ice floe; X = location of the river reach; and a,b = empirical constants. The parameter t_i is included for the reason that the roughness of a flat ice cover formed by the accumulation of frazil and brash ice will increase with the size and roughness of ice floes.

The increase in n_i during the decay period of the ice season is represented by the component n_t in the simulation model. This component is assumed to be a linear function of time. For the upper St. Lawrence River, the first day to have the effect of n_t was found to be the first day in the late winter to have an average daily temperature rising above 27^oF. Let this day be defined as t_b. The functional form n_t is then

$$n_t = 0 \qquad \text{for } t \leq t_b \tag{74}$$

$$n_t = s_n(t-t_b) \qquad \text{for } t \geq t_b \tag{75}$$

where, s_n is a constant which may vary depending on the location and year.

The fluctuating component, $\tilde{n}$, is considered to be governed by the transport and deposition of frazil ice. This component can be obtained from the following empirical relationships.

$$\tilde{n} = \kappa A_o T_a U^{-\tau} \qquad \text{for } t < t_F \tag{76}$$

$$\tilde{n} = \kappa A_o (T_a + T_r) U^{-\tau} \qquad \text{for } t_F \leq t \tag{77}$$

in which, T_a = average mean daily air temperature of the three preceeding days in terms of the freezing degree-days, ^{o}F-day; T_r = a reference temperature; U = average of the flow velocity of the day under consideration and that of the preceeding day in fps; A_o = open water area within or immediately upstream of the study reach; κ and τ = empirical constants. Application of the model to reaches of the upper St. Lawrence River (108) shows parameters λ, γ, δ, τ, and κ are site independent, although the ice cover condition varies substantially along the river. Values of these constant parameters are presented in Table 5.

Table 5. Empirical Constants of the Resistance Model for the Upper St. Lawrence River (108)

Empirical Constant	Estimated Value
λ	2
γ	0.5
δ	2
τ	11 when U < 1.9 fps 9 when U > 1.9 fps
κ	0.01

Hydraulic Analysis of Ice-Covered Rivers

With the existence of an ice cover, the head loss in a river channel will increase significantly over that of open water conditions at an equivalent discharge. This increase in

head loss, which is caused by the increase in wetted perimeter and the displacement effect of the floating cover, often leads to an increase in water level. If the resistance coefficient of the ice cover is known, then conventional backwater or unsteady flow computation techniques can be applied to Eqs. 52 and 53 to determine discharge distribution and water surface profiles in rivers and channel networks. Examples of these computational models include those of Calkins et al. (28), Pasquarell (68), and Yapa (108).

Stage-Discharge Relationships.

One important aspect of river engineering is to obtain accurate stream flow data at selected gaging stations. The stage-discharge relationship at a given gaging station developed for open water conditions is not suitable for ice-covered conditions. Cook and Cerny (33) and Rosenberg and Pentland (76) discussed gaging techniques used in the United States and Canada. With adequate winter data at a gaging station a stage-discharge relationship may be developed. The accuracy is much poorer due to the changing resistance of the ice cover related to the variations of the ice cover roughness and the frazil ice accumulation. Hirayama (47) proposed a procedure for estimating a stage-discharge relationship for ice-covered rivers with no unstable frazil ice accumulation. In this method the winter stage is related to the summer stage of equal discharge by Eq. 78

$$A_i R_i^{2/3} = K A_o R_o^{2/3} \qquad (78)$$

in which, S = channel slope; A = flow cross sectional area; R = hydraulic radius; i and o = subscripts representing ice-covered and open water conditions, respectively. The coefficient is defined as

$$K = \frac{n_c}{n_b} \left(\frac{S_o}{S_i}\right)^{1/2} \tag{79}$$

The coefficient K varies as a function of time during a winter. Based on field data a typical curve for K can be constructed and used in Eq. 78 to determine the winter discharge from the winter stage and the summer stage-discharge curve. Figure 15 shows the variation of K for a typical river.

Ice Jam Stage.

In cold regions, many flood events are ice-related. Most severe ice-related flood events are those caused by ice jams due to their large thickness and hydraulic resistance. A practical problem related to this is to estimate the stage caused by an ice jam given channel geometry and flow discharge. Using Eq. 49, Beltaos (17) obtained an expression for the stage, H_j, of an equilibrium ice jam as the following:

$$\eta = 0.63 f_c^{1/3} \xi + \frac{5.7}{\mu} \{1+[1+0.11\mu \frac{f_i}{f_c^{2/3}} \xi]^{1/2}\} \tag{80}$$

in which, $\eta = H_j/(S_o B)$; $\xi = (q^2/gS_o)^{1/3}/S_o B$; $f_c = (f_i+f_b)/2$; f_i, f_b = friction factor of the ice cover and the channel bed, respectively; S_o = channel slope; B = top width of the flow cross section; $q = Q/B$; Q = flow discharge. Since Eq. 80 is

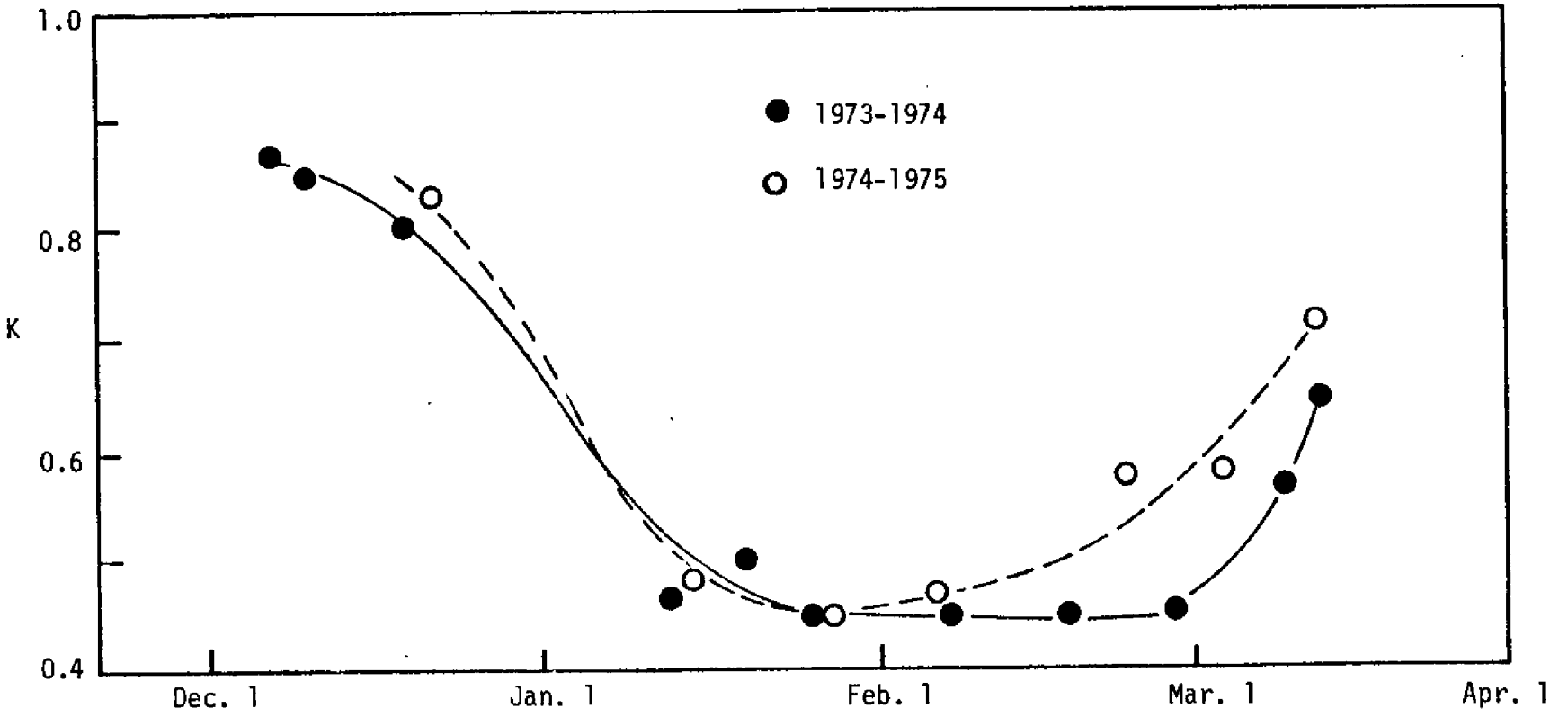

Figure 15. Seasonal change of coefficient K at Mukawa Gaging Station, Hokaido, Japan (47).

weakly dependent on f_i and f_c, a standard curve can be developed with some field data for the relationship between dimensionless stage, η, and dimensionless discharge, ξ, as shown in Figure 16. Gerard and Calkins (42) incorporated a similar method into flood frequency analysis and developed a method for constructing synthetic flood stage probability distribution curves of rivers in cold regions.

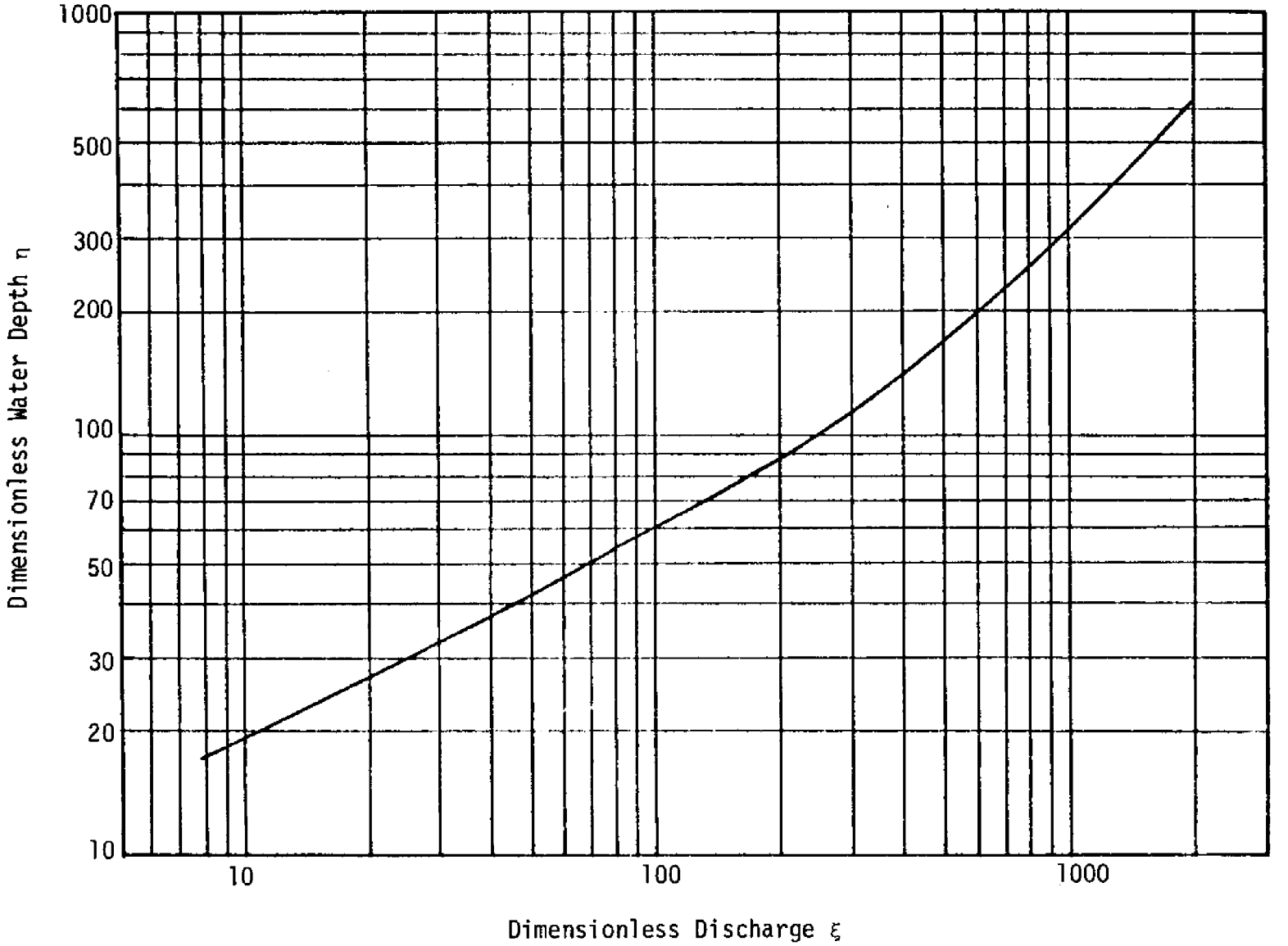

Figure 16. Dimensionless water depth due to an equilibrium, floating wide channel jam vs. dimensionless discharge (17).

VI. DETERIORATION AND BREAKUP OF ICE COVER

Early in the spring or late in the winter, especially after the disappearance of the snow cover, the ice cover melts from both its top and bottom surfaces and disintegrates from inside. This deterioration process causes rapid reduction in the strength of the ice cover and hence its load carrying capacity. The breakup of ice cover is a phenomena contributed by both the deterioration of the ice cover and the increase in discharge (18,37,56). Ice jams formed during the breakup and the accompanying flooding is a major cause of concern in many northern rivers.

Ice-Cover Deterioration

The thermal growth and decay of river ice cover has been discussed in Chapter II. Methods for determining the reduction in ice cover thickness were presented. In this section, deterioration or the weakening of the internal structural integrity of ice cover will be discussed.

The phenomena of ice cover deterioration is commonly observed early in the spring. During this period, the internal melting of ice at boundaries of crystal grains by the penetrated solar energy will lead to the loss of strength. Bulatov (20) considered the melting of the ice cover by short-wave penetration and established that the strength of melting ice is dependent on its liquid content. Ashton (10) developed a similar ice deterioration model independent of Bulatov. In Ashton's model the melting of the ice cover is analyzed by considering the combined radiation-conduction heat transfer.

The water content is determined by solving the unsteady heat conduction equation, Eq. 33, in the intact portions of the ice cover. The strength of the ice cover is then related to the porosity e_m by considering the reduction in effective contact area between grains. The relationship is

$$\frac{\sigma_i}{\sigma_o} = 1 - 2.813e_m \tag{79}$$

in which, e_m = porosity in the ice cover due to internal melting; σ_i = failure stress; and σ_o = failure stress when e_m is zero. Ashton also suggested that the elastic modulus will decrease with the increase in porosity. Based on studies in sea ice, the following linear relationship was postulated.

$$E/E_o = 1 - e_m/e_o \tag{80}$$

in which, E = Young's modulus; E_o = values of E when e_m is zero; and e_o = value of the porosity when E is zero.

Breakup of Ice Cover

The timing of breakup is of importance in the planning of ice-related operations such as the scheduling of a navigation season, the planning of hydropower production, and the assessment of the severity of the potential river flood associated with breakup jams. Breakups can generally be categorized into two types: "overmature" breakup and "premature" breakup (18,37,56). The overmature breakup is a slow process due to the deterioratoin of the ice cover by radiation-conduction heat transfer until it can gradually

disintegrate in place by frictional and gravitational forces. This type of breakup often occurs in controlled rivers and is known to cause relatively little negative impact on the river reach. The premature breakup is a faster and more drastic process occuring as a result of a substantial increase in river discharge caused either by intensive snowmelt or rainfall during a warm period. With an increase in discharge, the ice cover first fractures in fast steep sections, breaks into pieces and moves downstream to accumulate at the upstream end of still intact ice sheets. This process forms ice jams, which can be analyzed by theories of ice cover progression as discussed in Chapter IV. A continuous warming trend and increase in discharge will lead to successive fractures of ice sheets. This will lead to the shifting of existing ice jams downstream to form even larger jams. The flood stage during a premature breakup increases with the size of jam until the final ice run clears the ice in the channel (56).

The initiation of breakup in a river is influenced by ice cover conditions, weather conditions, flow conditions and the morphology of the river channel (91). Shulyakovskii (92) formulated an analytical model for the initiation of breakup assuming the ice cover is already separated from the river banks with a water level higher than the maximum winter freezeup level, H_F. The initiation of the breakup is defined as the instant when the strength of the cover is exceeded and transverse cracks form. By considering the force and moment acting on the ice cover, the breakup is shown to initiate when

$$\sigma_i\theta = f_1 (H_B - H_F , H_F) \quad (81)$$

Beltaos (16,18), extended this model and shows that

$$H_B/H_F = f_2 (\theta/W_F , \sigma_i/\tau_i, \text{dimensionless constants}) \quad (82)$$

in which, θ = ice cover thickness; H_B and H_F = average depth associtaed with flows breakup initiation and freezeup; W_F = maximum freezeup width of the cover during the winter; τ_i = shear stress on the underside of the cover due to flow. Field data shows that H_B/H_F increases with the value of θ/W_F. Beltaos further shows that there exists an ice clearing discharge q_c, which has an upper limit depending on θ, σ_i, H_F, τ_i and channel geomorphology.

$$q_c^* + \frac{1.59}{f_c^{1/3}} \left(\frac{\rho_i}{\rho} \frac{\theta}{H_F}\right) \leq \frac{1.59}{f_c^{1/3}} f\left(\frac{\theta}{W_F}, \text{other dimensionless river constants}\right) \quad (83)$$

in which, q_c^* = dimensionless ice clearing discharge, $q_c^{2/3}/((gs)^{1/3}Y_F)$; s = channel slope; f_c = composite friction factor of the flow under the cover. Equation 81 is confirmed by field data, which shows that q_c increases with θ/W_F. Based on the conceptual model of Beltaos, methods for forecasting the initiation of breakup were developed with moderate success using hydrometric station records (15,97).

VII. SUMMARY

In this report, a review of various aspects of the hydraulics and ice processes in rivers is given. A great deal of progress has been made by researchers in this field in the last two decades. It is expected that the understanding on many of the subjects discussed will be improved in the near future. A number of subjects are not covered in this review. These include field observation techniques; river ice controls; inland winter navigation; dispersion in ice covered rivers; and sediment transport under ice conditions.

NOTATION

The following is a list of symbols which are often used in this report:

A = flow cross sectional area;

A_s = surface area of a river reach;

A_{sn} = mass rate of snow fall;

B_c = width of the ice cover;

C = Chezy's Coefficient;

C_c = cloud cover in tenths;

C_i = frazil ice concentration;

c_i = specific heat of ice, 1.0 cal g^{-1} $^oC^{-1}$;

C_p = specific heat of water, 1.0 cal g^{-1} $^oC^{-1}$;

d_w = depth of flow;

E = Young's modulus;

E_x = longitudinal dispersion coefficient;

e = porosity of ice floe;

e_a = vapor pressure at the temperature T_a;

e_p = porosity in the ice accumulation between ice floes;

e_s = saturated vapor pressure at the temperature T_s;

F_r = Froude number upstream of the leading edge of the ice cover $V/\sqrt{gH}$;

F_{rc} = critical Froude number for juxtaposition;

F_{rc} = critical Froude number for ice cover progression;

f_i, f_b = friction factors of the ice cover and channel bed, respectively;

H = depth of the flow upstream of an ice cover;

H_e = water level, $z+d_w+\bar{h}_i$;

H_u = flow depth under an ice jam;

h_i = initial ice cover thickness;

$\bar{h}_i$ = equivalent thickness of the ice cover;

h_{ia} = energy exchange coefficient at the air-ice interface;

h_{wa} = energy exchange coefficient at the air-water interface;

h_{wi} = heat transfer coefficient for q_{wi};

k_i, k_b = roughness heights of the ice cover and the channel bed, respectively;

k = thermal conductivity of ice;

k_t = the composite roughness height;

k_w = thermal conductivity of water;

L = under-cover travel distance of an ice floe;

L_i = latent heat of fusion of ice 80 cal g^{-1};

ℓ_i = horizontal dimension of ice floe;

N_u = Nusselt Number, $h_{wi}R/k_w$;

n = Manning's coefficient;

n_c = composite Manning's coefficient;

n_i, n_b = Manning's coefficients of the ice cover and the channel bed, respectively;

P_r = Prandtl Number $\rho\nu_w C_p/k_w$;

p_i, p_b = wetted perimeter formed by the channel bed and the ice cover;

Q = river discharge;

Q_i^s = surface ice discharge;

q_{gw} = bed heat influx;

q_{wi} = heat flux from water to ice;

R = hydraulic radius;

R_e = Reynolds Number, UR/ν_w;

S = cumulative freezing degree-days;

T = Temperature in ice cover;

T_a = air temperature;

T_f = freezing point, 0^oC;

T_s = temperature at the surface of the river;

T_w = water temperature;

T_y = a time period of one year;

T_{ak} = air temperature in ^{o}k;

T_{sk} = surface temperature in ^{o}k;

t_i = thickness of ice floe;

U = flow velocity under an ice cover;

V = velocity upstream of an ice cover;

V_a = wind velocity;

V_p = visibility;

V_s = velocity of surface ice floes;

V* = shear velocity;

V_{cp} = velocity of progression of the leading edge of the ice cover;

z_b = bed elevation;

α = albedo;

$\Delta\rho$ = $\rho-\rho_i$;

ε = emissivity;

θ = ice cover thickness;

ν_w = kinematic viscosity of water;

ρ = density of water;

ρ_i = density of ice;

σ = Stefan-Boltzman constant;

σ_i = failure stress of the ice cover;

τ_i, τ_b = shear stress at the channel bed and the ice cover, respectively;

Φ = latitude in degrees;

ϕ = angle of friction of granular ice mass;

ϕ_b = long wave radiation flux;

ϕ_c = sensible heat exchange;

ϕ_e = evapo-condensation flux;

ϕ_p = penetrated short wave radiation;

ϕ_r = heat exchange due to precipitation;

ϕ_s = net solar radiation flux

REFERENCES

1. Ackermann, N.L. and Shen, H.T., Mechanics of surface ice jam formation in river. CRREL Report 83-31, U.S. Army Cold Regions Research and Engineering Laboratory, Hanover, N.H., 1983, 14 p.

2. Arden, R.S., and Wigle, T.E., "Dynamics of Ice Formation in the Upper Niagara River," The Role of Snow and Ice in Hydrology, Unesco-WMO-IAHS, Sept. 1972, pp. 1296-1313.

3. Ashton, G.D. and Kennedy, J.F., "Ripples on Underside of River Ice Covers," Journal of the Hydraulics Division, Vol. 98, No. HY9, Sept. 1972, pp. 1603-1624.

4. Ashton, G.D., "Froude Criterion for Ice-Block Stability," Journal of Glaciology, Vol. 13, No. 68, 1974, pp. 307-313.

5. Ashton, G.D., "Movement of Ice Floes Beneath a Cover," Technical Note, U.S. Army CRREL, Hanover, N.H., Feb. 1975.

6. Ashton, G.D., "River Ice," Annual Review of Fluid Mechanics, Vol. 10, 1978, pp. 369-392.

7. Ashton, G.D., "Suppression of River Ice by Thermal Effluents," CRREL Report 79-30, Cold Regions Research and Engineering Lab., U.S. Army, Hanover, N.H., Dec., 1979, 23 p.

8. Ashton, G.D., "Freshwater Ice Growth, Motion, and Decay," in Dynamics of Snow and Ice Masses, S.C. Colebeck, ed., Academic Press, 1980, pp. 261-304.

9. Ashton, G.D., "Theory of Thermal Control and Prevention of Ice in Rivers and Lakes," Advances in Hydroscience, Vol. 13, 1982, pp. 131-185.

10. Ashton, G.D., "Deterioration of Floating Ice Covers," Third International Symposium on Offshore Mechanics and Arctic Engineering, New Orleans, 1984.

11. Ashton, G.D., (ed.), River and Lake Ice Engineering, IAHR, 1985, In Press.

12. Barnes, H.T., Ice Engineering, Renouf Publishing Co., Montreal, 1928, 364 p.

13. Bates, R.E., and Bilello, M.A., "Defining the Cold Regions of the Northern Hemisphere," Technical Report No. 178, U.S. Army Cold Regions Research and Engineering Lab., Hanover, N.H., 11 p.

14. Beltaos, S., and Dean, A.M., "Field Investigations of a Hanging Ice Dam," Vol. I, International Symposium on Ice, Quebec City, Canada, 1981, pp. 475-488.

15. Beltaos, S., "Study of River Ice Breakup using Hydrometric Stations Records," Workshop on Hydraulics of River Ice, Fredericton, N.B., June 1981, pp. 41-64.

16. Beltaos, S., "Initiation of River Ice Breakup," Proc. Fourth Northern Research Basin Symposium Workshop, Norway, March 1982, pp. 163-177.

17. Beltaos, S., "River Ice Jams: Theory, Case Studies, and Applications," Journal of the Hydraulics Division, ASCE, Vol. 109, No. 10, Oct. 1983, pp. 1338-1359.

18. Beltaos, S., "River Ice Breakup," Canadian Journal of Civil Engineering, Vol. 11, Sept. 1984, pp. 516-529.

19. Bilello, M.A., "Maximum Thickness and Subsequent Decay of Lake, River, and Fast Sea Ice in Canada and Alaska," CRREL Report 80-6, U.S. Army Cold Regions Research and Engineering Laboratory, Hanover, N.H., 1980, 160 p.

20. Bulatov, S.N., "Calculating the Strength of Thawing Ice Cover and the Beginning of Wind-Activated Ice Drift," Trudy Vypysk 74, 1970, 120 p.

21. Bolsenga, S.J., "Total Albedo of Great Lakes Ice," Water Resources Research, Vol. 5, No. 5, Oct., 1969, pp. 1132-1133.

22. Brocard, D.N., and Harleman, D.R.F., "One-Dimensional Temperature Predictions in Unsteady Flows," Journal of the Hydraulics Division, ASCE, Vol. 102, No. HY3, Mar., 1976, pp. 227-240.

23. Calkins, D.J., "Accelerated Ice Growth in Rivers, CRREL Report 79-14, Cold Regions Research and Engineering Lab., Hanover, N.H., May 1979, 4 p.

24. Calkins, D.J., "Ice Cover Melting in a Shallow River," Canadian Journal of Civil Engineering, Vol. 11, 1984, pp. 255-265.

25. Calkins, D.J., "Numerical Simulation of Freeze-up on the Ottauquechee River," Workshop on the Hydraulics of River Ice, Fredericton, N.B., June 1984, pp. 247-277.

26. Calkins, D.J., and Ashton, G.D., Arching of fragmented ice covers, Canadian Journal of Civil Engineering, Vol. 2, No. 4, 1975, pp. 392-399.

27. Calkins, D.J., Deck, D.S., and Martinson, G.R., "Resistance Coefficients from Velocity Profiles in Ice-Covered Shallow Streams," Canadian Journal of Civil Eng., Vol. 9, No. 2, 1982, pp. 236-247.

28. Calkins, D.J., Hayes, R., Daly, S.F., and Montalvo, A., "Application of HEC-2 for Ice-Covered Waterways," Journal of the Technical Councils of ASCE, Vol. 108, No. TC2, Nov. 1982, pp. 241-248.

29. Carey, K.L., "Observed Configuration and Computed Roughness of the Underside of River Ice, St. Croix River, Wisconsin," Prof. Paper 550-B, U.S. Geological Survey, 1966, pp. B192-B198.

30. Carstens, T., "Experiments with supercooling and ice formation in flowing water," Geofysiske Publikasjoner, Vol. 26, No. 9, 1966, pp. 3-18.

31. Carstens, T., "Heat exchanges and frazil formation," in Proceedings of the Symposium on Ice and Its Action on Hydraulic Structures, Reykjavik, Iceland, International Association for Hydraulic Research, 1970, Paper No. 2.11.

32. Chow, V.T., Open-Channel Hydraulics, McGraw-Hill Book Co., 1959, 680 p.

33. Cook, R.E., and Cerny, E.E., "Patterns of Backwater and Discharge on Small Ice Affected Streams," U.S. Geological Survey Water Supply Paper 1892, pp. 114-125.

34. Daly, S.F., "Frazil Ice Dynamics," CRREL Monograph 84-1, U.S. Army Cold Regions Research and Engineering Laboratory, Hanover, N.H., April 1984, 46 pp.

35. Daly, S.F., "Ice Block Stability," Water for Resources Development, ASCE, Coeur d'Alene, Idaho, Aug. 1984, pp. 544-548.

36. Deck, D., "Controlling River Ice to Alleviate Ice Jam Flooding," Water for Resources Development, ASCE, Coeur d'Alene, Idaho, Aug. 1984, pp. 524-528.

37. Deslauriers, C.E., "Ice Break-Up in Rivers, Ice Pressure Against Structures," TM No. 92, National Research Council, Associate Committee on Geotechnical Research, Ottawa, Mar. 1968, pp. 217-230.

38. Dingman, S.L., and Assur, A., "The Effect of Thermal Pollution on River Ice Conditions - Part I, A Simplified Method of Calculation," CRREL Report 206, Cold Regions Research and Engineering Lab., U.S. Army, Hanover, N.H., 1967, 10 p.

39. Filippov, A.M., "Modeling the Movement of Ice Floes Drawn in Under Ice Cover," Translation TL473, U.S. Army CRREL, Hanover, N.H., 1974.

40. Gerard, R., "The Hydraulic Resistance of Ice Covers and Ice Jams: Some Reflections," Proceedings of Workshop on Hydraulic Resistance of River Ice, Burlington, Ontario, pp. 296-298.

41. Gerard, R., and Andres, D., "Hydraulic Roughness of Freeze-up Ice Accumulations: Northern Saskatchewan River Through Edmonton," Proceedings of the Workshop on Hydraulics of Ice-Covered Rivers, Edmonton, Alberta, June 1982, pp. 62-87.

42. Gerard, R., and Calkins, D.J., "Ice-Related Flood Frequency Analysis: Application of Analytical Estimates," Proceedings, Third International Specialty Conference on Cold Regions Engineering, Edmonton, Alberta, April 1984, pp. 70-85.

43. Goodrich, L.E., "A Numerical Model for Calculating Temperature Profiles in an Ice Cover," Proceedings, Research Seminar Thermal Regime of River Ice, Tech. Memo, No. 14, National Research Council Canada, Jan. 1975, Ottawa, Canada, pp. 44-59.

44. Greene, G.M., "Simulation of Ice-Cover Growth and Decay in One-Dimensional on the Upper St. Lawrence River," NOAA TM ERL GLERL-36, Great Lakes Environmental Laboratory, Ann Arbor, MI, 1981, 82 pp.

45. Halabi, Y.S., Shen, H.T., Papatheodorou, T.S., and Briggs, W.L., "Transport and Accumulation of Frazil Ice Suspensions in Rivers," Fourth International Conference on Mathematical Modelling, Zurich, Switzerland, Aug. 1983, pp. 412-417.

46. Haynes, F.D., and Ashton, G.D., "Turbulent Heat Transfer in Large Aspect Channels," CRREL Report 79-13, Cold Regions Research and Engineering Lab., U.S. Army, May 1979, 5 pp.

47. Hirayama, K., "Characteristics of Ice Covered Streams in Connection with Water Discharge Measurements," IAHR Ice Symposium, Vol. 2, Lulea, Sweden, Aug. 1978, pp. 195-217.

48. Ho, C.-F., "Two-Dimensional Application of Ice Cover Progression Theories in a Large River," MS Thesis, Clarkson University, Potsdam, N.Y., In Progress.

49. Hopper, H.R. and Raban, R.R., "Hanging Dams in the Manitoba Hydro System," Proceedings of Workshop on Hydraulic Resistance of River Ice, Burlington, Sept. 1980, pp. 195-208.

50. Jumikis, A.R., Thermal Geotechnics, Rutgers University Press, New Brunswick, N.J., 1977.

51. Kivisild, H.R., "Hydrodynamical Analysis of Ice Floods," 8th IAHR Congress, Paper 23F, Montreal, Canada, Aug. 1959, pp. 23-F-1~30.

52. Krutskih, B.A., Gudkovic, A.M., and Sokolov, A.L., eds., Ice Forecasting Techniques for the Artic Seas, Amerind Publishing Co. Pvt. Ltd., New Delhi, India, 1976.

53. Larsen, P.A., "Head Losses Caused by an Ice Cover on Open Channels," Jour. Boston Soc. Civil Engineers, 1969, pp. 45-67

54. Larsen, P.A., "Hydraulic Roughness of Ice Covers," Journal of the Hydraulics Division, ASCE, Vol. No. HY1, Proc. Paper 9498, Jan. 1973, pp. 111-119.

55. Matousek, V., "Types of Ice Run and Conditions for their Formation," Ice Symposium 1984, IAHR, Hamburg, 1984, pp. 315-327.

56. Michel, B., "Winter Regime of Rivers and Lakes," Cold Regions Science and Engineering Monograph III-B1a, Cold Regions Research and Engineering Lab., U.S. Army, Hanover, N.H., Apr. 1971, 131 p.

57. Michel, B., Ice Mechanics, Les Presses de L'Universte Laval, Quebec, 1978, 499 p.

58. Michel, B., "Ice accumulations at freeze-up or break-up," IAHR Symposium on Ice Problems, Lulea, Vol. 2, 1978, pp. 301-317.

59. Michel, B., "Comparison of Field Data with Theories on Ice Cover Progression in Large Rivers," Canadian Journal of Civil Engineering, Vol. 11, 1984, pp. 798-814.

60. Michel, B., and Drouin, N., "Equilibrium of an underhanging dam at the LaGrande River," Report GCS-75-03-01, Universite d'Laval, 1975, 8 p.

61. Michel, B., and Drouin, M., "Courbes de remous sous les couverts de glace de la Grande Riviere, Canadian Journal of Civil Engineering, Vol. 8, 1981, pp. 351-363.

62. Nezhikhovskiy, R.A., "Coefficients of Roughness of Bottom Surface of Slush Ice Cover," Soviet Hydrology: Selected Papers, No. 2, 1964, pp. 127-148.

63. O'Neil, K., and Ashton, G.D., "Bottom Heat Transfer to Water Bodies in Winter," Special Report 81-18, Cold Regions Research and Engineering Lab., U.S. Army, Hanover, N.H., 1981.

64. Osterkemp, T.E., "Frazil Ice Formation: A Review," Journal of the Hydraulics Division, ASCE, Vol. 104, No. HY9, 1978, pp. 1239-1255.

65. Paily, P.P., Macagno, E.O., and Kennedy, J.F., "Winter-Regime Surface Heat Loss from Heated Streams," IIHR Report No. 155, Iowa Institute of Hydraulic Research, Iowa City, Iowa, Mar. 1974, 137 pp.

66. Pariset, E. and Hausser, R., "Formation and Evolution of Ice Covers on Rivers," Transactions, Engineering Institute of Canada, Vol. 5, No. 1, 1961, pp. 41-49.

67. Pariset, E., Hausser, R., and Gagnon, A., "Formation of Ice Covers and Ice Jams in Rivers," Journal of the Hydraulics Division, ASCE, Vol. 92, Nov. 1966, pp. 1-24.

68. Pasquarell, G.C., "Flow Distribution in Ice Covered Channel Networks," M.S. Thesis, Clarkson College, Potsdam, N.Y., 1983.

69. Perovich, D.K., and Grenfell, T.C., "A Theoretical Model of Radiative Transfer in Young Sea Ice," Journal of Glaciology, Vol. 28, No. 99, 1982, pp. 341-356.

70. Petryk, S., and Boisvert, R., "Simulation of ice conditions in channels," Proceedings of the Specialty Conference on Computer Applications in Hydrotechnical and Municipal Engineering, Toronto, 1978, pp. 239-259.

71. Petryk, S., Panu, U., and Clement, F., "Recent improvements in numerical modelling of river ice," International Symposium on Ice, IAHR, Quebec, Vol. 1, 1981, pp. 426-435.

72. Petryk, S., Panu, U., Kartha, V.C., and Clement, F., "Numerical modelling and predictability of ice regime in rivers," International Symposium on Ice, IAHR, Quebec, Vol. 1, 1981, pp. 436-449.

73. Petukhov, B.S., and Popov, V.N., "Theoretical Calculation of Heat Exchange and Frictional Resistance in Turbulent Flow in Tubes of an Incompressible Fluid with Variable Physical Properties," High Temperature, Vol. 1, No. 1, 1963.

74. Pivorarov, A.A., Thermal Conditions in Freezing Lakes and Rivers, John Wiley & Sons, Inc., New York, N.Y., 1973, 135 p.

75. Pratte, B.D., "Review of Flow Resistance of Consolidated Smooth and Rough Ice Covers," Canadian Hydreological Symposium: 79, Proceedings, Vancouver, May 1979, pp. 52-92.

76. Rosenberg, H.B., and Pentland, R.L., "Accuracy of Winter Streamflow Records," Proceeding, Eastern Snow Conference, Hartford, Connecticut, Feb. 1966, pp. 51-72.

77. Rouse, H., Elementary Mechanics of Fluids, John Wiley Sons, Incv., 1946, p. 217.

78. Shen, H.T., "Surface Heat Loss and Frazil Ice Production in the St. Lawrence River," Water Resources Bulletin, Vol. 16, No. 6, 1981, pp. 996-1001.

79. Shen, H.T., "Hydraulic Resistance of River Ice," Frontiers in Hydraulic Engineering, ASCE, Cambridge, MA, 1983, pp. 224-229.

80. Shen, H.T., "Mathematical modeling of river ice process," Water for Resource Development, ASCE, Coeur d'Alene, Idaho, 1984, pp. 554-558.

81. Shen, H.T., and Ackermann, N.L., "Winter Flow Distribution in River Channels," Journal of the Hydraulics Division, ASCE, Vol. 106, No. HY5, May 1980, pp. 805-817.

82. Shen, H.T., and Ruggles, R.W., "Winter Heat Budge and Frazil Ice Production in the Upper St. Lawrence River," Water Resources Bulletin, Vol. 18, No. 2, Apr. 1982, pp. 251-257.

83. Shen, H.T., VanDeValk, W.A., "Field Investigation of St. Lawrence River Hanging Ice Dams," IAHR Ice Symposium, Hamburg, Aug. 1984, pp. 241-250.

84. Shen, H.T., Ruggles, R.W., and Batson, G.B., "Field Investigation of St. Lawrence River Hanging Ice Dams, Winter of 1983-84," Report DTSL55-84-C-C0085A, U.S. Department of Transportation, Washington, D.C., Aug. 1984, 85 p.

85. Shen, H.T., and Yapa, P.D., "Simulation of the Undersurface Roughness Coefficient of River Ice Cover," Report 82-6, Department of Civil and Environmental Engineering, Clarkson University, 98 p.

86. Shen, H.T., and Yapa, P.D., "A Unified Degree-Day Method for River Ice Cover Thickness Simulation," Canadian Journal of Civil Engineering, Vol. 12, 1985, pp. 54-62.

87. Shen, H.T., Foltyn, E.P., and Daly, S.F., "Forecasting Water Temperature Decline and Freeze-up in Rivers," CRREL Report 84-19, U.S. Army Cold Regions Research and Engineering Laboratory, Hanover, N.H., July 1984, 17 p.

88. Shen, H.T., and Chiang, L.A., "Simulation of growth and decay of river ice cover," Journal of Hydraulic Engineering, ASCE, Vol. 110, No. 7, July 1984, pp. 958-971.

89. Shen, H.T., and Yapa, P.D., "Computer Simulation of Ice Cover Formation in the Upper St. Lawrence River," Workshop on Hydraulics of River Ice, Fredericton, N.B., June 1984, pp. 227-246.

90. Shishokin, S.A., "Investigation of the Bouguer-Lambert Formula for the Penetration of Solar Radiation into Ice," Soviet Hydrology: Selected Papers, Vol. 3, 1969, pp. 287-295.

91. Shulyakovskii, G.L., Manual of Forecasting Ice-Formation for Rivers and Inland Lakes, Israel Program for Scientific Translation Ltd., Jerusalem, 1966, 245 p.

92. Shulyakovskiy, L.G., "On a Model of the Ice Breakup," Soviet Hydrology: Selected Papers, No. 1, 1972, pp. 21-27.

93. Simon, Li, and Associates, Engineering Analysis of Fluvial Systems, 1982, pp. 6.1-6.35.

94. Simonsen, C.P.S., and Carson, R.W., "Ice processes during construction of limestone generating station," Proceedings of the Third International Hydrotechnical Conference, Quebec City, 1977.

95. Starosolszky, O. (ed.), "Multilingual Ice Terminology," Internaitonal Association for Hydraulic Research, Research Center for Water Resources, Budapest, 1977 and 1980.

96. Starosolszky, O., "Ice in Hydraulic Engineering," Report 70-1, Norwegian Institute of Technology, Trondheim, 1969, 165 pp.

97. Tang, P.W., and Davar, K.S., "Forecasting the Initiation of Ice Breakup on the Nashwaak River," Workshop on Hydraulics of River Ice, Fredericton, N.B., June 1984, pp. 65-94.

98. Tatinclaux, J.-C., "Equilibrium Thickness of Ice Jams," Journal of the Hydraulics Division, ASCE, Vol. 103, No. HY9, Sept. 1977, pp. 959-974.

99. Tatinclaux, J.-C., and Gogus, M., "Stability of Floes Below a Floating Cover," Vol. 1, Internal Symposium on Ice, Quebec City, Canada, 1981, pp. 298-311.

100. Tatinclaux, J.-C., and Gogus, M., "Asymmetric Plane Flow with Application to Ice Jams," Journal of Hydraulic Engineering, ASCE, Vol. 109, No. 11, Nov. 1983, pp. 1540-1554.

101. Tsang, G., and Beltaos, S., Proceedings of Workshop on Hydraulic Resistance of River Ice, Environment Canada, Burlington, Canada, 1980, 301 pp.

102. Uzuner, M.S., "The Composite Roughness of Ice Covered Streams," Journal of Hydraulic Research, Vol. 13, No. 1, Jan. 1975, pp. 79-101.

103. Uzuner, M.S. and Kennedy, J.F., "Stability of Floating Ice Blocks," Journal of the Hydraulics Division, ASCE, Vol. 93, No. HY12, Dec. 1972, pp. 2117-2133.

104. Uzuner, M.S., and Kennedy, J.F., "Theoretical Model of River Ice Jams," Journal of the Hydraulic Division, ASCE, Vol. 102, Sept. 1976, pp. 1365-1383.

105. U.S. Army Corps of Engineers, "Ice Engineering," Engineering Manual, EM1110-2-1612, Washington, D.C., Oct. 1982.

106. Wake, A., and Rumer, R.R., Jr., "Modeling Ice Regime of Lake Erie," Journal of the Hydraulics Division, ASCE, Vol. 105, No. HY7, July 1979, pp. 827-844.

107. Wigle, T.E., "Investigation into Frazil, Bottom Ice and Surface Ice Formation in the Niagara River," IAHR Symposium on Ice and Its Action on Hydraulic Structures, Reykjavik, Iceland, Sept. 1976, paper 2.8.

108. Yapa, P.D., "Unsteady Flow Simulation of Rivers with an Ice Cover," Thesis presented to Clarkson College, at Potsdam, N.Y., in 1983, in partial fulfillment of the requirements for the degree of Doctor of Philosophy.

109. Yapa, P.D., and Shen, H.T., "Roughness Characteristics of the Upper St. Lawrence River," XXth Congress of the IAHR, Moscow, U.S.S.R., September 1983.